UNIVERSITÀ DEGLI STUDI
DI MILANO

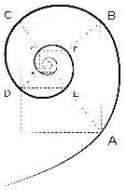

DOTTORATO IN MEDICINA MOLECOLARE E TRASLAZIONALE

CICLO XXXII

Anno Accademico 2018/2019

TESI DI DOTTORATO DI RICERCA

MED/04

^{99m}Tc-radiolabeled Nanoparticles for targeted detection and treatment of HER2-positive Breast Cancer

Dottorando: DR. PAOLO RAINONE

Matricola: R11762

Tutore: PROF.SSA MARIA ALFONSINA DESIDERIO

Co-Tutore: DR.SSA SARA BELLOLI

Coordinatore: PROF. MICHELE SAMAJA

Abstract

Introduction: *The HER2 receptor overexpression is normally associated to aggressive and infiltrating breast cancer (BC) phenotype with propensity to spread into metastases. Nowadays, the detection of HER2 in primary tumor lesions and in their metastases is based on invasive methods as well therapy clinical outcomes are not satisfactory yet. Recent advances in nanotechnology have led to the development of nanoparticles able to host various functionalities for specific targeting and to be loaded with therapeutic molecules, making possible the simultaneous diagnosis and treatment of human cancers (theranostic). In the present Thesis study, was evaluated the potential use of targeted silica nanoparticles (SiNPs) as theranostic agent for* $HER2^{+}$ *breast cancer.*

Methods: *SiNPs were engineered with anti-HER2 monoclonal antibody Trastuzumab, in the form of half-chain (Hc-TZ), and radiolabeled employing* ^{99m}Tc *for in vivo SPECT imaging detection of* $HER2^{+}$ *BC lesions. Subsequently, SiNPs were loaded with doxorubicin (DOX) for treatment evaluation. Experimental design was divided in three main tasks. First, we evaluated the contribution offered by active targeting (Hc-TZ) to the selective distribution of SiNPs in solid HER2 positive BC lesions. To this aim, both Hc-TZ conjugated (SiNP-TZ) and non-conjugated (SiNP) nanosilica shells were radiolabeled with* ^{99m}Tc*-Tricarbonyl complex, through nitrilotriacetic acid (NTA) linker procedure, and their distribution kinetics evaluated in vitro and ex vivo in ad hoc cancer models. Nanoparticles were simultaneous filled with a fluorescent dye and their uptake were also assessed by FACS analysis and fluorescence microscopy. In the second experimental step, nanoparticles were also engineered with several amount of Hc-TZ (SiNPs to Hc-TZ ratio, 1:2 and 1:8 respectively), and were* ^{99m}Tc*-labeled at histidine residues of the antibody chain for ex vivo/in vivo biodistribution evaluation.*

Finally, SiNP-TZ were loaded with DOX and in vitro/in vivo DOX distribution in HER2 positive models was evaluated using confocal microscopy and Optical Imaging, in comparison to liposomal doxorubicin (Caelyx). The treatment efficacy of DOX-SiNP-TZ (1:8 Hc-TZ) versus Caelyx was evaluated in vivo for six weeks of treatment, also using PET molecular imaging ([^{18}F]FDG) approach.

Results: *In vitro assays showed a higher fluorescence signal (FICT) in SK-BR-3 compared to MDA-MB-468 cells, exclusively for targeted SiNP-NTA-TZ/SiNP-TZ with an increase over time. Ex vivo biodistribution of ^{99m}Tc-labelled nanoparticles via NTA, at 4 h post-injection of SiNP-NTA-TZ and/or non-targeted (SiNP-NTA), exhibited values of 3.53 and 1.69 in tumor (tumor to muscle ratio) respectively, with a rapid reduction over time for targeted nanoparticles. These results indicated the presence of an antibody-receptor mediated tumor uptake of SiNP-NTA-TZ, with a faster washout of nanoparticles radiolabeled shell. In the second set of experiments, performed with ^{99m}Tc-SiNP-TZ labelled on TZ half chain, uptake was confirmed at 4 h p.i. for SiNP-TZ (1:8 Hc-TZ) with similar results to SiNP-TZ (1:2 Hc-TZ). Instead, was showed a progressive retention of radioactivity until 24 h p.i., confirming the presence of radiolabeled Hc-TZ to the tumor also at latter times, with improved results for SiNP-TZ (1:8 Hc-TZ), also in terms of radiochemical yield. Doxorubicin loaded SiNP-TZ (1:8 Hc-TZ) showed in vivo similar delivery results in comparison to Caelyx at 6 h p.i., meanwhile at the end of treatment tumor volume reduction resulted significant improved by targeted nanoparticles administration.*

Conclusion: *Results of this Thesis study, demonstrated a promising specificity and treatment efficacy of the silica nanoparticles-based system SiNP-TZ, encouraging its potential use as theranostic agent for HER2^{+} breast cancer lesions.*

Sommario

Introduzione: *La sovraespressione del recettore HER2 è solitamente associata ad un fenotipo di carcinoma mammario altamente aggressivo ed infiltrante, con propensione allo sviluppo di metastasi. Ad oggi, il rilevamento dell'espressione di HER2 nelle lesioni tumorali primarie ed in quelle metastatiche si basa su metodi invasivi, e gli esiti clinici dei trattamenti terapeutici non sono ancora soddisfacenti. I recenti progressi nelle nanotecnologie hanno portato allo sviluppo di nanoparticelle in grado di ospitare differenti funzionalizzazioni per il targeting specifico e di essere caricate con molecole chemioterapiche, rendendo possibile allo stesso tempo sia la diagnosi che il trattamento dei tumori (teragnostica). Nel presente elaborato di Tesi è stato valutato l'utilizzo di nanoparticelle in silice (SiNPs) come potenziale agente teragnostico per carcinoma mammario HER2 positivo.*

Metodi: *Le SiNPs sono state funzionalizzate con l'anticorpo monoclonale anti-HER2 Trastuzumab, utilizzando metà catena anticorpale (Hc-TZ), e sono state radiomarcate con l'isotopo ^{99m}Tc per il rilevamento in vivo delle lesioni tumorali HER2^{+}, mediante l'imaging SPECT. Successivamente, le nanoparticelle sono state caricate con doxorubicina (DOX) per valutarne l'efficacia di trattamento. Il design sperimentale è stato diviso principalmente in tre fasi. Innanzitutto, è stato valutato il contributo offerto dalla funzionalizzazione delle SiNPs con Hc-TZ (rapporto SiNPs:Hc-TZ, 1:8) al targeting selettivo delle lesioni HER2 positive. A tal fine, nanoparticelle funzionalizzate con Hc-TZ (SiNP-TZ) e non (SiNP), sono state radiomarcate con il complesso ^{99m}Tc-Tricarbonyl attraverso la procedura che utilizza la presenza dell'acido nitrilotriacetico (NTA) come linker, sui rispettivi gusci in silice. La loro cinetica di distribuzione è stata valutata in vitro ed ex vivo in modelli tumorali ad hoc. Inoltre, le SiNPs sono state riempite con un fluoroforo (FITC), ed il loro assorbimento è stato anche valutato mediante*

analisi FACS e microscopia a fluorescenza. Nella seconda fase sperimentale, le SiNPs sono state progettate con diverse quantità di Hc-TZ (rapporto SiNPs:Hc-TZ, 1:2 e 1:8 rispettivamente) e sono state ^{99m}Tc-marcate sui residui di istidina presenti sulla catena anticorpale, per la valutazione della loro biodistribuzione ex vivo/in vivo. Infine, le SiNP-TZ (1:8 Hc-TZ) sono state caricate con DOX per valutarne la diffusione in vitro e in vivo in modelli tumorali HER2 positivi, mediante microscopia confocale e imaging ottico, rispetto all'utilizzo di doxorubicina liposomale (Caelyx). L'efficacia di trattamento delle DOX-SiNP-TZ è stata valutata in vivo per sei settimane di trattamento, in confronto alla somministrazione i.v. di Caelyx, anche mediante l'imaging molecolare PET ([^{18}F]FDG).

Risultati: *I test di fluorescenza in vitro hanno mostrato un segnale più elevato (FICT) nella linea cellulare SK-BR-3 (HER2^{+}) rispetto alle cellule MDA-MB-468 (HER2^{-}), esclusivamente quando incubata con le nanoparticelle funzionalizzate SiNP-NTA-TZ/SiNP-TZ, con un progressivo aumento nel tempo. La biodistribuzione ex vivo delle SiNPs radiomarcate con ^{99m}Tc via NTA, a 4 h post-iniezione di SiNP-NTA-TZ o SiNP-NTA, ha mostrato valori di assorbimento di 3.53 e 1.69 nel tumore (rapporto tumore-muscolo) rispettivamente per le due varianti, con una rapida riduzione a tempi successivi osservata per le nanoparticelle funzionalizzate SiNP-NTA-TZ. Questi risultati potrebbero essere indice della presenza di un assorbimento tumorale specifico mediato dal legame anticorpo-recettore da parte delle SiNP-NTA-TZ, con un'eliminazione più rapida del guscio in silice radiomarcato. Nella seconda serie di esperimenti, eseguita con ^{99m}Tc-SiNP-TZ radiomarcate a livello dei residui di istidina sulla Hc-TZ, l'assorbimento è stato confermato a 4 h p.i. per le SiNP-TZ (1:8 Hc-TZ), con risultati simili a quelli mostrati dalle SiNP-TZ (1:2 Hc-TZ). A tempi successivi, invece, è stato mostrato un progressivo aumento della radioattività, confermando la presenza al tumore della catena anticorpale (Hc-TZ) radiomarcata fino a 24 h p.i., con risultati maggiori per le SiNP-TZ (1: 8 Hc-TZ), anche in termini di*

resa radiochimica. La doxorubicina veicolata dalle SiNP-TZ (1: 8 Hc-TZ) ha raggiunto in vivo valori di diffusione tumorale simili al Caelyx a 6 h p.i., mentre al termine del trattamento ha mostrato un aumento significativo nella riduzione del volume tumorale.

Conclusioni: *I risultati ottenuti nel presente elaborati di Tesi, hanno dimostrato una promettente specificità ed efficacia di trattamento da parte del sistema a base di nanoparticelle in silice SiNP-TZ (1: 8 Hc-TZ), promuovendo il suo potenziale utilizzo come nuovo agente teragnostico per il carcinoma mammario HER2 positivo.*

Index

1. Introduction

1.1. Breast Cancer

Breast cancer (BC) is the most frequently occurring cancer in women, and it represents the second cause of cancer.[1] The natural history of BC commonly implies the progression from primary pre-neoplastic lesions to invasive carcinomas, finally involving to metastatic lesions.[2] Worldwide in 2018, nearly 2 million of new cases of BC occurred and caused the death of about 600,000 of women.[3] While mortality rates decreased by 14% since 2008, the incidence of BC worldwide increased by more than 20% with about 1.7 million new cases each year, accounting for 25% of all cancer cases.[4] Overall, BC is the second leading cause of mortality after the lung cancer, and it has long been the leading cause of cancer death among women. Despite important advances in research, BC incidence and mortality degree are supposed to increase significantly in the next 5–10 years.[5] Diagnosis and screening are usually performed by anatomic imaging technics as X-Ray mammography (gold standard), Computed tomography, Magnetic Resonance Imaging (MRI) and echography.[6] Molecular imaging technics such as Positron Emission Tomography (PET) and Single Photon Emission Computerized Tomography (SPECT), were recently introduced only for staging and follow up, with promising diagnostic application and phenotypical assessment.[7] BC patients are usually subject to multimodality treatment that involves surgery, radiation therapy and drug therapy.[4] The first two modalities are mainly used for treatment of the primary lesions, but their efficacy decrease with cancer progression and metastasis,[8] stressing the

relevance to develop new effective and safe treatment strategies for this prevalent and deadly malignant disease. Due to the unsatisfactory improvement in both survival rate and toxicity reduction for most cancer types by standard systemic chemotherapy (as the gold-standard approach), the scientific community and the money investments by the pharmaceutical industry have been attracted by the nanomedicine and targeted therapy.[9] Nevertheless, the chemotherapy resistance and the substantial improvement in survival rates remain the main problem and represent the mains researchers' goals. Moreover, the phenotypic/genotypic heterogeneity of neoplastic populations within a patient's tumor, and among different patients, are features that can complicate diagnosis and challenge treatment setting. Tumor heterogeneity complicates correct diagnosis, and a single biopsy might prejudge the complexity of the disease. Different histopathological biomarkers, such as receptor expression (estrogen-receptor, progesterone-receptor and/or HER2/ERBB2), contribute to diagnostic classification,[10] and molecular profiling subdivides BC into at least five subtypes as reported in Figure 1 (triple negative or basal like, HER2 overexpressing, luminal A, luminal B and normal like).[11] Treatment planning, prognosis and responses to therapy reflect these expression profiles.[12] Clinically, this tumor heterogeneity is subdivided into three main therapeutic groups. The Estrogen Receptor (ER) positive group is the most wide (luminal A and luminal B), and in order to predict the outcomes for ER patients receiving endocrine therapy several genomic tests are needed.[13] The HER2/ERBB2 overexpressing group has shown the main clinical success, due to efficacy of immuno-therapeutic targeting of the receptor.[14] Triple

Negative BCs (TNBC) and the remaining subtypes have only chemotherapy options.[15]

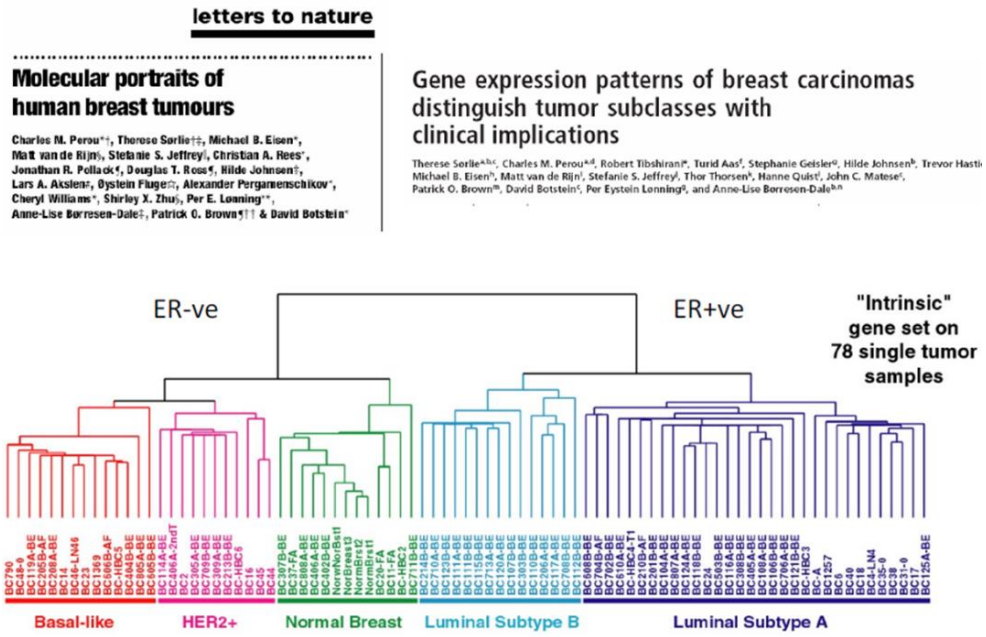

Figure 1. Gene expression patterns of experimental samples representing 78 breast carcinomas. The tumor specimens were divided into five subtypes based on differences in gene expression. The cluster dendrogram showing the five subtypes of tumors are colored as: luminal subtype A, dark blue; luminal subtype B, light blue; normal breast-like, green; basal-like, red; and ERBB2+, pink.[16,17]

The succeeding greater problem is usually the tumor staging, i.e., as the disease spread. The primary tumor within the breast (stage 1), frequently invade the tissues and lymph nodes nearest (stage 2–3) or the distant organs (distant metastasis, stage 4).[15] The most frequent sites of metastasis spread are bone, lung, liver and brain.[18] Therefore, in order to have a benefit from related therapies, the detection of tumor phenotype remains a fundamental issue. Nowadays, biomarkers

expression is evaluated through invasive techniques, on post-surgery or biopsy specimen by immunohistochemistry (IHC) or fluorescence in-situ hybridization (FISH), and it is performed ordinarily on the primary lesion.[19] Staging and search for metastases is only needed in symptomatic patients, or in those at high risk for relapse. The prevalence of metastasis in asymptomatic patients is high in large tumors or in patients with extensive nodal disease.[20] Routine staging examinations consist of chest radiography, abdominal ultrasound, and bone scan.[7] New advances in PET/SPECT molecular imaging techniques, as well as the identification of new biomarkers and the development of their radiochemistry, could overcome to limitations associated with anatomical imaging techniques and the invasiveness of biopsy sampling.

1.2. HER2 positive breast cancer

1.2.1. Human epidermal growth factor receptor 2 (HER2)

Human epidermal growth factor receptor 2 (HER2/ERBB2), a transmembrane tyrosine kinase (TK), plays a critical role in the triggering of the downstream signaling cascades that control cell proliferation, survival, and apoptosis in BC.[21] It is well known that HER2 gene is amplified in about 30% of BC patients, and that it is associated with aggressive phenotype and poorer clinical outcome,[22] making HER2 an intriguing target for both diagnosis and therapy.[23] Generally, the HER/ERBB proteins undergo dimerization upon ligand (EGF, EPR, TGFα, etc.) binding to their extracellular domains, with transphosphorylation of their intracellular domains: in BC HER2 is the predominant TK receptor.[24] HER2 does not have a ligand and relies

on heterodimerization with another family member or homodimerization with itself when expressed at very high levels, to be activated (Fig. 2).[25] Intracellular phosphorylated tyrosine residues crosstalk with several intracellular signaling proteins, leading to activation of downstream second messenger pathways. Transcription factors activated by these pathways modulate many genes involved in cell proliferation, survival, differentiation, angiogenesis, invasion and metastasis.[26] HER2 has higher catalytic kinase activity than the other HER family members, and HER2 forming heterodimers have the strongest signaling activity.[27] Anti-HER2 monoclonal antibodies, such as Trastuzumab (TZ) and Pertuzumab, can be directly used to avoid the triggering of HER2 signaling with an important benefit. TZ and Pertuzumab monoclonal antibodies show high affinity of binding to two different extracellular domains of HER2 receptor, hampering its homodimerization or heterodimerization, respectively (Fig. 3).[28,29]

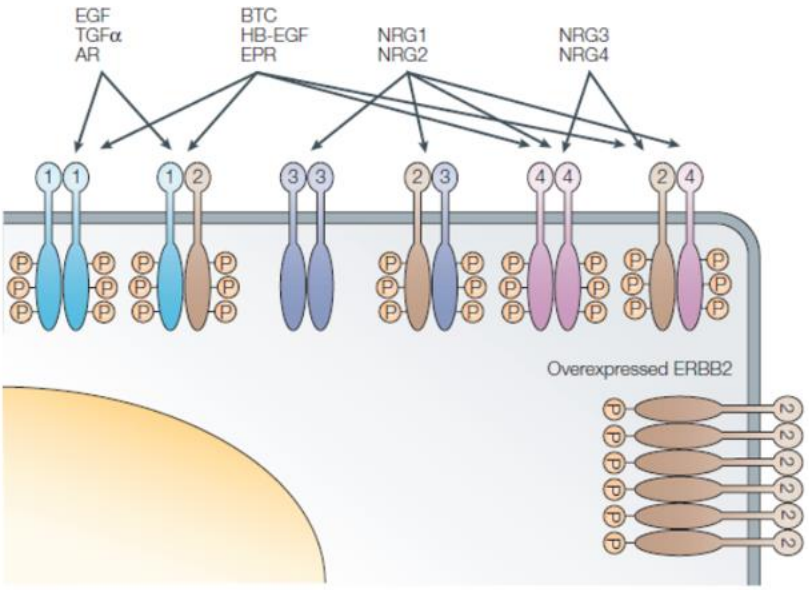

Figure 2. ERBB family and cell signaling: ligand binding to domains I and III of EGFR/HER1, HER3 and HER4 leads to homo/heterodimer formation, receptor internalization, kinase activation and downstream signaling. No known ligand binds directly to HER2, nevertheless its overexpression lead to homodimerization.[25]

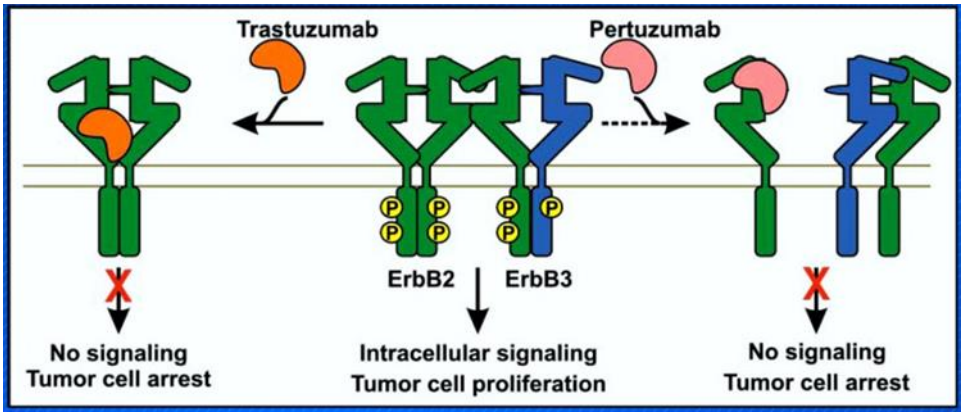

Figure 3. Treastuzumab and Peruzumab mechanisms of action and intracellular signaling. Trastuzumab and Pertuzumab, have a different mode

of action on ErbB signaling. Trastuzumab (on the left) is a humanized monoclonal antibody to subdomain IV of ErbB2. This leads to disruption of ErbB2-ErbB2 complexes signaling, formed when ErbB2 is overexpressed, and in absence of ligand-binding. The mechanisms of this disruption are still unclear. Disruption of these complexes inhibits PI3K signaling and Akt activation and explains the antiproliferative effects of Trastuzumab in ErbB2-amplified tumor cells. Effects of trastuzumab on ligand-induced dimerization of ErbB receptors seem minor or absent. Pertuzumab (on the right) is a humanized monoclonal antibody to subdomain II, the dimerization arm of ErbB2. Pertuzumab leads to inhibition of ligand-induced ErbB2 signaling, not of ligand-independent ErbB2 signaling.[30]

1.2.2. Therapy

The development of Trastuzumab (TZ), a recombinant humanized monoclonal antibody able to recognize the extracellular domain of the HER2 protein, has drastically revised the natural history of HER2-positive ($HER2^+$) BC, and ranks among the most significant advances in cancer therapeutics.[31] TZ was originally approved for use in HER2 positive metastatic BC by the United States Food and Drug Administration (FDA) in 1998, based on a randomized phase III study, where the combination of TZ and chemotherapy (anthracyclines or taxanes) in previously untreated patients significantly improved objective response rates, progression free survival, and general survival compared to chemotherapy alone.[23] Moreover the addition of Pertuzumab,[28] a recent HER2-directed monoclonal antibody, to neoadjuvant TZ plus Docetaxel significantly increased the proportion of patients achieving a pathological complete response, compared with TZ plus Docetaxel. This lead to the approval of neoadjuvant TZ

and Pertuzumab plus the taxane (Docetaxel) chemotherapy in the USA, European Union, and other countries.[32] However, several studies on women receiving anthracycline (doxorubicin) for the treatment of BC showed that TZ and taxanes (Paclitaxel) are highly active at aggravating the cardiac and systemic toxicity.[33] In order to overcome the chemotherapy toxicity problems, the development of Nanomedicine has offered several advantages. Until today, only few nanomedicine products have obtained US Food and Drug Administration (FDA) approval: Doxil (liposomal doxorubicin) and Abraxane (Albumin conjugate to Paclitaxel) are the two most successful nanoformulations already widely used for BC treatment in clinical settings.[34,35] In any case, recurrence and disease progression degree remain dramatically high. The new drug TZ emtansine (T-DM1), an antibody cytotoxic drug conjugated, has improved overall survival in patients with HER2-positive metastatic BC, who were previously treated with TZ and a taxane. FDA approved T-DM1 as monotherapy for the treatment of patients with HER2-positive advanced BC, who had previously received TZ and taxane in 2013.[36,37] The safety and efficacy of this novel agent in BC field, notwithstanding its limitation in the treatment of metastatic HER2-positive BC, has been further assessed recently.[36] Nevertheless, in order to have a benefit from TZ or related therapies, the detection of HER2 expression remains a fundamental issue, reachable preferentially by noninvasive and full body scan techniques.

1.3. Diagnosis and staging

1.3.1. Molecular imaging

Molecular and anatomical imaging is a branch of biomedical sciences including tomographic techniques such as PET (positron emission tomography), SPECT (single photon emission computerized tomography), CT (computed tomography), MRI (magnetic resonance imaging) and non-tomographic techniques like US (ultrasounds) for the study and the characterization of molecular and morphological processes in living organisms under normal and pathological conditions.[38] Even if, these techniques allow with some limitations to study specific molecular targets or tissues characteristics, and their changes over time and the different pathological stages. For these reasons, the research is focused on the selection of suitable molecules (probes) to obtain an image of the biological/pathological process under study. These probes need specific characteristics to reach the target of interest, including the capability to cross biological barriers like vessels' walls, interstitial and cellular membranes as well as the capability to stay in circulation for the time necessary to interact with the target, before to be excreted and degraded. Moreover, essential properties for the probe are low immunogenicity and absence of pharmacological effect by itself. The most used techniques to obtain molecular information from biological systems are PET/SPECT imaging,[39] allowing the study of cellular metabolism and biochemical reactions within the organism in physiological and pathological conditions. These techniques are based on the use of molecules involved in biomolecular processes, radiolabeled through gamma emitting radioisotopes.[40] The use of these probes *in vivo* permits to

evaluate their distribution and behavior in the different biological district, discriminating pathological changing in noninvasive way.

1.3.2. Breast cancer and imaging

Nowadays, detection and staging of BC is performed by anatomical techniques, such as X-Ray mammography (gold standard), CT and US, meanwhile phenotype assessment is based on immunohistochemical analysis on biopsy specimens from primary lesion and regional lymph nodes (Fig. 4).[7] The advances of next-generation technologies, that could provide quantitative imaging biomarkers for diagnostic and therapeutic monitoring of HER2-positive (HER2+) disease in BC patients, have been widely promoted as an effective approach for renewal oncological care,[41] although numerous hurdles have been met. Despite various conventional imaging modalities, such as MRI, US, and CT, show potential in terms of improving the diagnostic specificity of X-ray mammography screening,[7] no imaging technique alone, to date, can achieve high enough detection sensitivity and specificity to significantly impact the management of this disease. PET/SPECT imaging have progressed to improve their sensitivity and accuracy for the identification of several tumor biomarkers, such as HER2 in primary and metastatic lesion. Several studies have reported consistent results through the use of radiolabeled antibody.[42] Radionuclide-based imaging techniques can be exploited to visualize and quantify the presence/absence of biological markers by means of specific radiolabeled probes, administered at tracer dose.[43] Hence, these techniques may allow the assessment of HER2 expression both in primary and secondary lesions not accessible with the biopsy.[44] To this aim, new advances in

Nanomedicine offer innovative radiolabeled probes, which show various functionalities in order to improve specificity and sensitivity versus the target, and offer multilabeling chance for multimodal imaging diagnostic techniques.[45] Among the radionuclides currently used in nuclear medicine for radiolabeling, ^{99m}Tecnetium (^{99m}Tc) offers a favorable half-life (about 6 h) to follow *in vivo* distribution of labeled molecules, with several advantages in terms of radioprotection (optimal gamma ray energy emission, 140 keV) and availability, thanks to the local presence of clinical grade generators.[46]

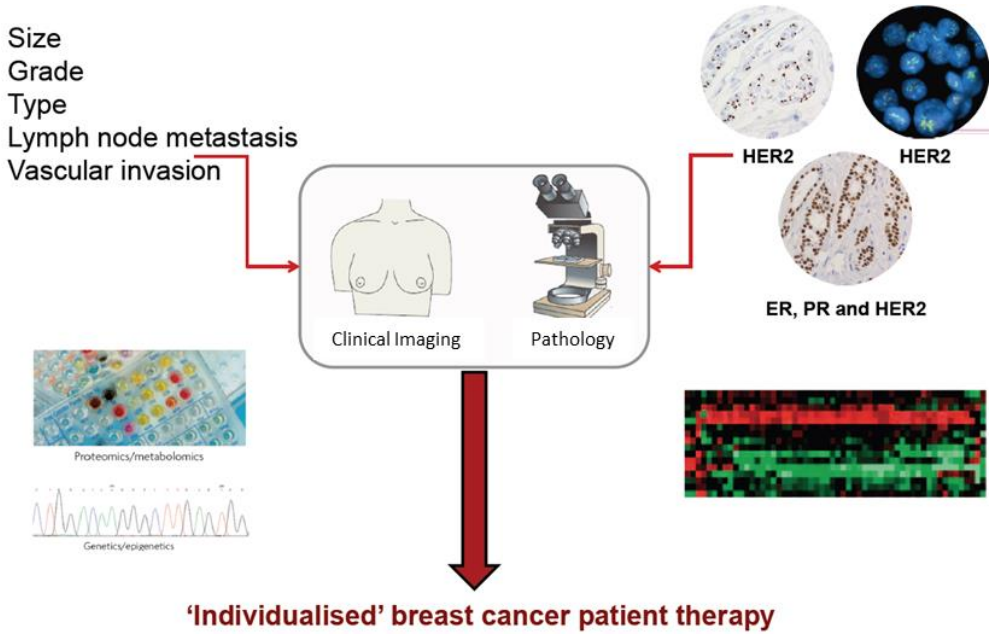

Figure 4. Schematic illustration of breast cancer diagnosis staging and treatment planning in clinical setting. The patient with breast cancer is first clinically staged, which results in a clinical TNM-stage. Treatment planning is then discussed in a multidisciplinary team. In many patients, surgery will be the next step. Increasingly, neoadjuvant chemotherapy is given in order to decrease the tumor burden prior to surgery. Following surgery or biopsy, the specimens (tumor, sentinel node or axillary nodes after dissection) are

analyzed by the pathologist. On this results in a pathology TNM-stage the post neoadjuvant therapy is added, further treatment with adjuvant chemotherapy, radiotherapy and hormonal or HER-2 targeted therapy is discussed in the multidisciplinary team.

1.4. Nanomedicine

Nanomedicine, the application of nanotechnology to achieve breakthroughs in healthcare, is one of most promising new therapeutic options in oncology. By definition, nanotechnology is the branch of technology that deals to application and engineering of materials with dimensions and tolerances below 100 nanometres, although devices of 100–200 nm are often considered nanomedicine in practice.[47] Nanocarriers models range from liposomes, nanotubes, micelles, dendrimers, nanoparticles (NPs) and so on, and they can be composed of several materials such as phospholipids, lipids, proteins, polymers, inorganic materials or a mixture of this (Fig. 5).[48] Some formulations are already commonly introduced in clinical treatment of BC with positive results: they are liposomes (eg, Doxil®) and nanoparticles (eg, Abraxane® and T-DM1®).[49] Nevertheless, these products were initially realised as generic anticancer drug carriers. Recently, with a better interpretation of molecular biology of BC, several promising tailored nanodelivery strategies are actively explored. It should be noted that nanomedicine can provide a wide range of benefits for cancer patients besides treatment, including disease detection, cancer imaging and tissue repairing.[49]

The study reported in my Doctoral Thesis has focused mainly on the diagnostic and treatment aspect, with emphasis on the advanced use of targeted radiolabelled NPs with the capaibility to carry anticancer

agents. Targeted NPs are a powerful drug delivery systems, since they can enhance the potency of chemotherapy drugs improving the diffusion within tumor cells overexpressing antigens such as HER2,[50] with a reduction of toxicity for healthy cells.[51] In general, NPs can easily cross the tumor vessels, and are retained in the tumor due to the enhanced permeability and retention (EPR) effect.[52] However, this passive diffusion is not enough to limit their delivery exclusively to cancer cells.[53] Various ligands can offer specificity of binding to receptors overexpressed in cancer cells, such as peptides, aptamers and antibodies. These molecules have been co-engineered with nanomaterials for the synthesis of innovative drug delivery systems and targeted diagnostic probes (theranostics).[54] Indeed, it is possible to label the NPs with radioactive and/or fluorescent probes for imaging detection, without affecting their therapy efficacy, meanwhile gaining high signal-to-background ratio.[55] Silica NPs (SiNPs) possess high biocompatibility, and their functionalization with monoclonal antibodies (*e.g.*, TZ for $HER2^+$ BC) can be a useful tool for both tumor imaging and targeted chemotherapy (theranostics).[44,56] Moreover, these NPs are hydrophilic, easy and inexpensive to prepare and can be chemically modified in a variety of ways.[57] SiNPs are optically transparent in the near-infrared (NIRF), and visible at ultraviolet region: these properties are particularly favorable for *in vivo* imaging application.[44,58] These reasons have recently induced the researchers to employ SiNPs as new probes in imaging studies, including PET/SPECT, MRI and/or fluorescence imaging, and at the same time as nanocarriers for targeted treatment of diverse kinds of cancer in preclinical studies.[59-61]

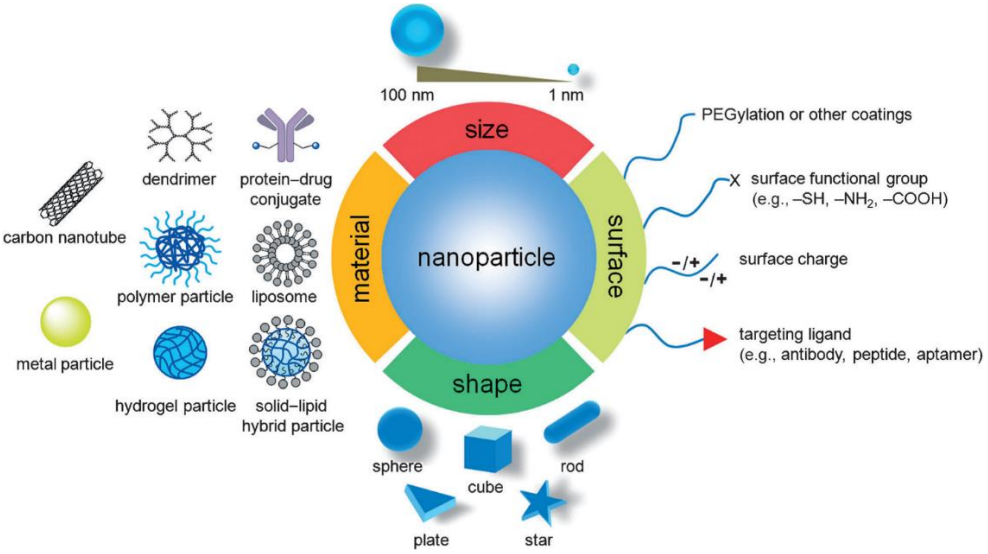

Figure 5. Engineered Nanoparticles for Drug Delivery in Cancer Therapy. The illustration reports the main materials and shapes employed for the synthesis as well as the size range and the most surface functionalization used in Nanomedicine.[62]

2. Aim of the study

In the experiments of this Thesis, we explored the use of multifunctional ^{99m}Tc-labelled SiNPs for early detection and treatment of HER2 positive BC lesions. For HER2+ tumor targeting, spherical SiNPs (hydrodynamic size ≈ 100 nm) were engineered with the half-chin (Hc) of TZ monoclonal antibody (or without Hc-TZ, as negative control), and were radiolabeled employing the radioisotope ^{99m}Tc. Then, engineered nanoparticles were used for *ex vivo* biodistribution profiling, and *in vivo* SPECT imaging evaluation, with an *ad hoc* animal models. During these specificity evaluation studies, nanoparticles were also engineered with several amounts of Hc-TZ (1:2 and 1:8, SiNPs to Hc-TZ ratio). Moreover, SiNPs were initially filled with the fluoresceine isothiocyanate (FITC) dye to allow their detection by fluorescence microscopy and flow cytometry in *in vitro/ex vivo* specificity assay. Subsequently, SiNPs were loaded with doxorubicin (DOX) to follow both the *in vitro* and *in vivo/ex vivo* drug delivery (confocal microscopy and optical imaging) and the treatment efficacy (tumor volume reduction and PET imaging), by comparing several nanoparticles formulations.

The aim of this work was to investigate the contribution offered by Hc-TZ active targeting to SiNPs biodistribution, for imaging application and in terms of treatment efficacy, using HER2+ BC models. For this end, we realized and tested two different radiolabeling strategies, through nitrilotriacetic acid (NTA) linker procedure or without it (i.e. direct procedure on histidine-residues of Hc-TZ): these strategies allowed to follow the nanoparticles tumor uptake and their distribution kinetics in peripheral districts, using nuclear medicine techniques. The

SiNPs system could be potentially used to develop a theranostic nanosystem combining noninvasive detection with an effective treatment for $HER2^{+}$ mammary cancer.

3. Material and methods

3.1. Synthesis and characterization of FITC loaded nanoparticles with nitrilotriacetic acid (NTA), SiNP-NTA and SiNP-NTA-TZ (1:8 Hc-TZ)

In the first part of the study, spherical nanoparticle shell was synthetized with nitrilotriacetic acid (NTA) liker, able to bind with high affinity the His-Tag-Tricarbonyl-complex (^{99m}Tc[CO]3)$^{+}$-His-Tag, in order to radiolabel and follow the nanoparticles shell, for either SiNPs with Hc-TZ (SiNP-NTA-TZ) or without (SiNP-NTA) by nuclear medicine techniques. SiNPs were initially filled with the fluoresceine isothiocyanate (FITC) dye to allow their *in vitro/ex vivo* detection by fluorescence imaging techniques. The reaction and characterization protocols were performed according to the method used in a recent study by Rainone *et al.*[44] SiNP-NTA-TZ was functionalized with a number of about eight Hc-TZ per nanoparticle, SiNP-NTA-TZ (1:8 Hc-TZ).

3.2. Synthesis and characterization of FITC loaded nanoparticles, with several amount of Hc-TZ (1:2 and 1:8 Hc-TZ) and without NTA linker SiNP-TZ

In order to perform further investigation, SiNP-TZ were synthetized without NTA for the radiolabelling by direct procedure; we also reduced the amount of Hc-TZ conjugated to the nanoparticle shell. During the synthesis of SiNP-TZ (1:2 Hc-TZ), the reaction protocols[43] was developed using a quarter of Hc-TZ dose, in comparison to SiNP-TZ (1:8 Hc-TZ).

3.3. Radiolabeling of SiNP-NTA and SiNP-NTA-TZ (1:8 Hc-TZ)

3.3.1. Step 1: Preparation of (^{99m}Tc[CO]$_3$)$^+$

The Isolink kit (Paul Scherrer Institut, Villigen, Switzerland) used to prepare the labeling precursor ([^{99m}Tc(H_2O)$_3$(CO)$_3$]$^+$), contained the following lyophilized ingredients: 8.5 mg sodium tartrate, 2.85 mg sodium tetraborate decahydrate, 7.15 mg of sodium carbonate and 4.5 mg sodium bicarbonate. Freshly eluted $^{99m}TcO_4^-$ from a commercial General Electric Healthcare, UK generator (~2 GBq), in 1 ml saline buffer was added to the kit vial, and incubated at 100°C for 20 min. The vial was then allowed to cool at room temperature (RT), and the solution was neutralized by adding stepwise 1M HCl to reach pH ~7 by checking on pH paper (Merck Millipore, Milan, Italy). The radiochemical purity (RCP) of the product was analyzed by high performance liquid chromatography (HPLC), and RPC was greater than 95%.

3.3.2. Step 2: (^{99m}Tc[CO]$_3$)$^+$-His-Tag prelabeling

An hexa-His-Tag peptide was prelabeled with (^{99m}Tc[CO]$_3$)$^+$. Conjugation of the hexa-His-Tag was almost quantitative and was performed by mixing 38 µL of peptide solution (5 mg/ml in Hepes buffer pH 7.4) to the ([^{99m}Tc(H_2O)$_3$(CO)$_3$]$^+$) precursor solution. The solution mixture was incubated at RT under stirring for 60 min; then the % RCP was checked by HPLC, and it was found to be greater than 95%.

3.3.3. Step 3: Conjugation of (^{99m}Tc[CO]$_3$)$^+$-His-Tag to SiNP-NTA

The (^{99m}Tc[CO]$_3$)$^+$-His-Tag solution was added to 500 µL of SiNP-NTA (6.7 mg/ml), using 4 nmol NTA/mg SiNPs. The solution mixture was

incubated at RT under stirring for 2.5 h, and then the % RCP was checked. The solution was shaken for about 1 min on a vortex mixer, and then centrifuged for 15 min at 18,000 rpm. Supernatant solution was withdrawn, and the corresponding radioactivity was counted. The pellet was washed with Hepes buffer and centrifuged three times. After the measurement of radioactivity of total supernatant and pellet the % RCP was 42%.

3.3.4. Step 4: Conjugation of (^{99m}Tc[CO]$_3$)$^+$-His-Tag to SiNP-NTA-TZ

The (^{99m}Tc[CO]3)+-His-Tag solution was added to 500 µL of SiNP-NTA-TZ NPs (8.6 mg/ml), using 4 nmol NTA/mg SiNPs. The solution mixture was incubated at RT under stirring for 2.5 h; then the % RCP was checked as described above, and it was 23.8%.

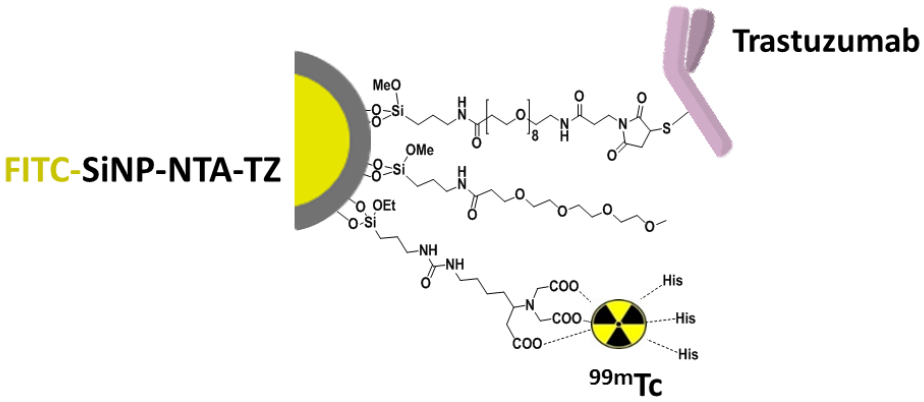

Figure 6. Illustration of FITC loaded nanoparticles ^{99m}Tc-SiNP-NTA-TZ, radiolabeled by NTA method on nanoparticles shell. FITC was loaded in nanoparticles core (yellow), the radioisotope ^{99m}Tc was introduced on NTA linker.

3.4. Radiolabeling of SiNP -TZ (1:2 and 1:8 Hc-TZ), without NTA linker

SiNP-TZ nanoparticles, realized without NTA linker, were radiolabeled directly on histidine (His) residues of Hc-TZ, in order to evaluate also the distribution of this component *in vivo/ex vivo* and for simplify the radiolabeling procedure. The SiNP-TZ radiolabeling was performed as described in the previous section, avoiding some steps: in $(^{99m}Tc[CO]_3)^+$-HisTag prelabeling, steps 2, and $(^{99m}Tc[CO]_3)^+$-His-Tag prelabeling step 3. During the step 4, conjugation of $(^{99m}Tc[CO]_3)^+$ was performed adding its solution to SiNP-TZ (1:2 and 1:8) under the same reaction conditions. RCPs checked as described above, were 24.6% and 19.8% for SiNP-TZ 1:2 and 1:8, respectively.

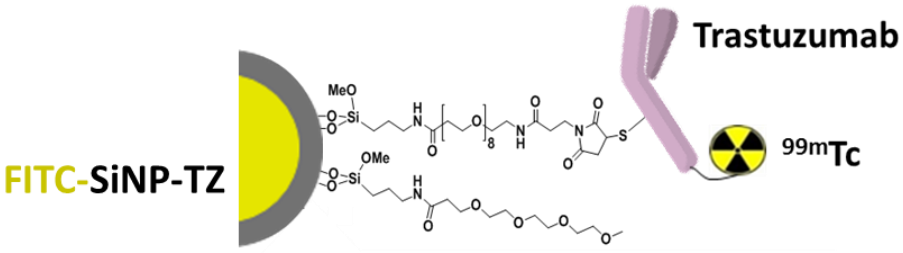

Figure 7. Illustration of FITC loaded nanoparticles ^{99m}Tc-SiNP-TZ, radiolabeled by direct method, on histidine residues expose on antibody chain of Hc-TZ.

3.5. Synthesis and characterization of doxorubicin externally loaded nanoparticles SiNP and SiNP-TZ (1:8 Hc-TZ)

For outside doxorubicin loaded nanoparticle, the synthesis protocol was performed according to the method used in a recent study by Riva *et al.*[63] In order to obtain the chosen amount of Hc-TZ conjugated to

the nanoparticles shell (1:8 Hc-TZ) the reaction protocol was developed as previously described for FITC loaded nanoparticles SiNP-TZ (1:8 Hc-TZ).

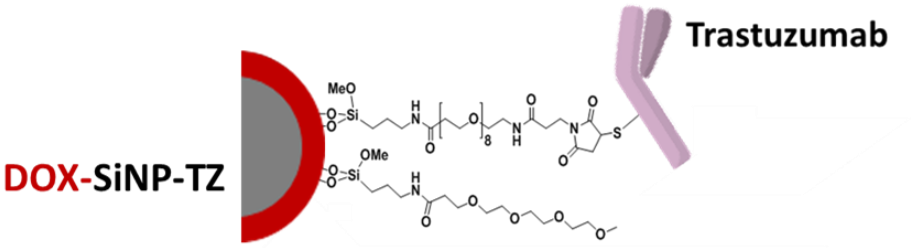

Figure 8. Illustration of doxorubicin externally loaded nanoparticles SiNP-TZ. Doxorubicin was loaded on nanoparticles' shell (red).

3.6. Cell culture

The uptake of silica nanoparticles was studied using SK-BR-3 ($HER2^+$) and MDA-MB-468 ($HER2^-$) cell lines (ATCC; USA). Confocal microscopy was also performed using MCF-10A (non-transformed mammary epithelial cells line) (ATCC; USA). MDA-MB-468 and SK-BR-3 cells were maintained in Dulbecco's Modified Eagles Medium high glucose (Sigma-Aldrich), supplemented with 5% penicillin/streptomycin, 10% heat-inactivated fetal bovine serum (Euroclone) and 2 mM L-glutamine. MCF-10A cells were cultured in Advanced DMEM medium (GIBCO) containing 10% heat-inactivated foetal bovine serum, 2mM L-glutamine, 100 U/ml penicillin and 100 mg/ml streptomycin, 10 µg/ml Insulin (Sigma-Aldrich), 20 ng/ml epidermal growth factor (EGF; Sigma-Aldrich) and 0.5 µg/ml Hydrocortisol (Sigma-Aldrich).

3.7. Animal models

Female Balb/c nude mice were obtained from the ENVIGO RMS S.r.l. Italy. Animal experiments were carried out in compliance with the institutional guidelines for the care and use of experimental animals (IACUC), which have been notified and approved by the Italian Ministry of Health and the Ethics Committee of the San Raffaele Scientific Institute (approval number 10/2016-PR). Balb/c nude mice with the age of 7–8 weeks and weight of 24–26 g were maintained under specific pathogen free condition. To obtain SK-BR-3 tumor models, about 5×10^6 cells in 200 µL mixed solution (serum-free RMPI-1640 medium and matrigel at the volume ratio of 1:1) were injected under the right shoulder. Calipers were used to measure tumor volume (mm^3) 2 times per week, and mice weight was recorded. Mice were randomized when tumor volumes reached an average of 100 mm^3.

3.8. In vitro binding specificity of FITC-SiNPs by flow cytometry

SK-BR-3 cells ($HER2^+$, 3×10^5) were incubated with 0.5 µg/ml of SiNP, SiNP-TZ (1:8 Hc-TZ), SiNP-NTA or SiNP-NTA-TZ (1:8 Hc-TZ) dispersed in serum free-DMEM. After different incubation times (20 min, 1 h, 4 h and 24 h), cells were washed twice with PBS, and harvested in fluorescence-activated cell sorting (FACS) tubes. A total of 10^5 events were acquired for each analysis on FACS Calibur flow cytometer (Becton Dickinson, Milan, Italy) monitoring FITC emission (green fluorescence). Both the percentage of the fluorescent cells relative to the control (untreated cells), and the mean fluorescent intensity of the fluorescence-positive cells were taken into account. The same experiment was performed with MDA-MB-468 cell line

(HER2$^-$), as a negative control. The results were analyzed using FlowJo software.

3.9. In vitro fluorescence microscopy of FITC-SiNPs

SK-BR-3 (HER2$^+$, 5×10^4) and MDA-MB-468 (HER2$^-$, 5×10^4) cells were grown on glass coverslip (diameter 3.5 cm) incubated with 0.025 mg of SiNP, SiNP-TZ (1:8 Hc-TZ), SiNP-NTA or SiNP-NTA-TZ (1:8 Hc-TZ) dispersed in cell culture media. After 20 min, 1 h, 4 h and 24 h of incubation at 37 °C (humidified atmosphere, 5% CO_2 air), the medium was removed and the cells were washed three times with PBS. The samples were fixed with methanol (at –20 °C for 30 min) before fluorescence analysis; cell nuclei were counterstained by Hoechst (Life Science) 1 µg/ml. The specific uptake of SiNPs in both cell lines was visualized by fluorescence microscopy (Nikon Eclipse 80i).

3.10. In vitro uptake of ^{99m}Tc-SiNPs-NTA, radiolabeled by NTA linker procedure

SK-BR-3 (HER2$^+$) and MDA-MB-468 (HER2$^-$) cells were cultured at a density of 5×10^4 cells per well in 24-well plastic dishes (Corning, USA) for 48 h. Then, the cell medium was removed, and 0.5 ml of DMEM supplemented with 10% FBS solution was added to each well. ^{99m}Tc-labeled SiNP-NTA or SiNP-NTA-TZ (1:8 Hc-TZ) suspensions (1 µCi/ml) were added to the plates in 0.5 ml of saline solution. The cells were then incubated at 37 °C for 1 h, 4 h and 24 h in a humidified atmosphere, with 5% CO_2. At the predicted times, the DMEM suspensions were collected and the cells were washed with 300 µL of PBS. Cell collection was performed using 200 µL of 0.05% Trypsin-

EDTA (1×) solution for 10 minutes. The radioactivity of the cells and of each removed solution were then measured using a γ-counter (LKB Compugamma CS 1282). The percentage of radioactivity in cells compared to the total radioactivity for each well was calculated.

3.11. Ex vivo biodistribution of ^{99m}Tc-SiNPs-NTA in the tumor, radiolabeled by NTA linker procedure

^{99m}Tc-labeled SiNPs were evaluated on HER2^{+} xenograft tumor model, prepared using Balb/c nude mice. Mice were anaesthetized with a mixture of 4 % isoflurane in air, and subdivided in two experimental groups. One group of 12 mice was injected in the tail vein with 100 µL of a solution containing ^{99m}Tc-labeled SiNP-NTA-TZ; the other group of mice was injected i.v. with non-targeted ^{99m}Tc-labeled SiNP-NTA (3.7 MBq/ml, pH~7.4). Additional aliquots, (0.1 ml) of both radioactive solution were diluted 1:10, 1:100 and 1:1000, and used to calculate the standard curve. Four animals per experimental point were sacrificed (at 4 h, 6 h and 24 h, post-injection) under general anesthesia (mixture of 4 % isoflurane in air). Tumor and muscle samples were removed and placed in vials for the count and the weight. Tissue samples and standards were placed in a γ-counter (LKB Compugamma CS 1282), and counts corrected for physical decay. The radioactivity concentration in tumor was calculated as percentage of injected dose per gram of tissue (%ID/g), and also expressed as tumor to muscle ratio.

3.12. Ex vivo fluorescence microscopy of ^{99m}Tc-SiNPs-NTA in tumor

After radioactivity count, tumor samples were fixed with 4% paraformaldehyde for 4 h, and embedded in optimal catting medium (OCT, Sakura Finetek, Torrance, CA), to prepare frozen sections. For immunofluorescent staining, tumor sections (10 μm) were rinsed with PBS, and blocked with 5% BSA for 60 min followed by the incubation with primary antibody (rabbit anti-β-Actin, diluted 1:50; Sigma Aldrich) overnight at 4 °C. The day after, tumor sections were washed for 5 min three times with PBS. Sections were then incubated with the secondary antibody (Alexa Fluor488-labeled goat anti-rabbit IgG, diluted 1:200; Sigma Aldrich) for 60 min at RT. After a rinse with PBS, the washed sections were incubated with 4-6-diamidino-2-phenylindole (DAPI) for 5 min. Finally, sections were sealed with anti-fluorescence quenching agent (Beyotime), and observed by fluorescence microscopy (Nikon Eclipse 80i).

3.13. Ex vivo biodistribution of ^{99m}Tc-SiNP-TZ (1:2 and 1:8 Hc-TZ) in tumor, radiolabeled by direct procedure

^{99m}Tc-labeled SiNPs were evaluated on HER2^{+} xenograft tumor model, prepared using Balb/c nude mice. Mice were anaesthetized with a mixture of 4 % isoflurane in air, and subdivided in two experimental groups. One group (17 mice) was injected in a tail vein with 100 μL of a solution containing ^{99m}Tc-labeled SiNP-TZ (1:8 Hc-TZ), and the other group (15 mice) with radiolabelled nanoparticles 1:2 Hc-TZ functionalized (37 MBq/ml, pH~7.4). Additional aliquot (0.1 ml) of both radioactive solution was diluted 1:10, 1:100 and 1:1000 and

used to calculate the standard curve. After the SiNPs injection, three animals per group were sacrificed at 1 h, six animals per 1:8 Hc-TZ group and five animals per 1:2 Hc-TZ group were sacrificed at 4 h. Five animals per 1:8 Hc-TZ group and three animals per 1:2 Hc-TZ group were sacrificed at 6 h, and three animals per 1:8 Hc-TZ group and four animals per 1:2 Hc-TZ group were sacrificed at 24 h. The sacrifice were done under general anesthesia. Tumor and muscle samples were removed and placed in counting vials for count and weigh. Tissue samples and standards were placed in a γ-counter (LKB Compugamma CS 1282), and counts corrected for physical decay. The radioactivity concentration in tumor was calculated as percentage of injected dose per gram of tissue (%ID/g) and also expressed as tumor to muscle ratio.

3.14. Explorative in vivo SPECT evaluation of ^{99m}Tc-SiNP-TZ in HER2^{+} mouse model

SPECT images were acquired with a YAP-(S)-PET II small animal scanner (ISE S.r.l., Pisa, Italy) in three dimensional mode, and reconstructed using the expectation maximization (EM) algorithm. This scanner is made up of four detector heads: each one is composed of a 4×4 cm^2 YAlO3:Ce (or YAP:Ce) matrix of 20×20 elements, (2×2× 25 mm^3 each), coupled to an R2486 PS-PMT (Hamamatsu). A high resolution collimator with parallel holes has been placed in front of the crystals for SPECT modality acquisition. The four modules are positioned on a rotating gantry. Our scanner is characterized by an axial field of view (FOV), and a diameter of the transaxial FOV of 4 cm. The spatial resolution is 5.2 mm^3 (full-width at half-maximum), and the maximum of absolute sensitivity measured in the center of the FOV is

1.87 % for 50–850 keV energy window. A female Balb/c nude mouse was anaesthetized with a mixture of 4 % isoflurane in air, and was injected intravenously with 6.5 MBq of radiolabelled ^{99m}Tc-SiNP-TZ (1:8 Hc-TZ). After 1, 4 and 24 hours of radiolabelled nanoparticles injection the mouse was positioned prone on the PET/SPECT scanner bed with the tumour centred in the field of view (FOV). Dynamic SPECT data were acquired for 30 minutes (six scans of 5 minutes). SPECT data were acquired in list mode, using the full axial acceptance angle of the scanner (3D mode), and then reconstructed with the Expectation Maximization (EM) algorithm. All images were calibrated with a dedicated phantom, corrected for the radionuclide half-life decay.

3.15. In vitro evaluation of cell internalization by doxorubicin loaded nanoparticles (DOX-SiNPs)

Subcellular localization of DOX was tested on SK-BR-3 (HER2$^+$ BC) and MCF-10A (HER2$^-$, non-transformed mammary epithelial) cells. SK-BR-3 and MCF-10A cells (5×10^4) were grown on glass coverslips, and cultured at 37 °C for 24 h. Then, the cells were incubated with DOX-SiNP or DOX-SiNP-TZ (1:8 Hc-TZ) nanoparticles at a DOX concentration of 1 μM for 1 h at 37 °C. Cells without treatment were used as control. Next, the medium was removed, and the cells were washed with PBS solution twice, followed by the treatment with antifade mounting Medium (with DAPI to stain the nucleus) for another 15 min. The subcellular distribution of DOX was recorded using a Leica laser scanning confocal microscope (TCS SP8 SMD FLIM).

3.16. In vivo and ex vivo evaluation of doxorubicin delivery by DOX-SiNPs and Caelyx

Female Balb/c nude mice were randomized when tumor volumes reached an average of 100 mm^3 and subdivided into three groups (3 mice per group), i.e. each one per a nanoparticles set. The tumor volume was calculated following the formula: $width^2$ X length/2. After general anesthesia, with a mixture of 4 % isoflurane in air, the mice of each group were intravenously injected with a nanoparticle solution containing 60 µg of DOX in different formulations: Caelyx (liposomal DOX) [20mg/ml]; DOX-SiNP [20 mg/ml]; DOX-SiNP-TZ (1:8 Hc-TZ) [20 mg/ml]. Fluorescent image of each mouse was obtained using an IVIS Spectrum *in vivo* imaging system at selected time points (1, 4 and 6 h), in order to follow DOX distribution into the tumor overtime. After 6 h, euthanasia was done under general anesthesia and main tissues were carefully excised for fluorescent imaging quantification.

3.17. In vivo evaluation of treatment efficacy of DOX-SiNPs and Caelyx

Female Balb/c nude mice were randomized when tumor volumes reached an average of 100 mm^3 and subdivided into four treatment groups (Control: n. 5 mice; Caelyx: n. 9 mice; DOX-SiNP: n. 6 mice and DOX-SiNP-TZ: n. 8 mice). Mice were weekly injected i.v. with a dose of 1mg/Kg of DOX loaded as several nanoparticles formulations, for six weeks of treatment. Ctrl group was injected with vehicle solution. Efficacy of treatment was assessed *in vivo* monitoring twice a week the tumor volumes by digital Calliper. Tumor volume was calculated following the formula: $width^2$ X length/2, and percentage of

volume reduction was normalized per the first measure. Moreover, treatment efficacy was assessed evaluating glucose tumor metabolism. For this, [^{18}F]FDG tumor uptake was monitored by *in vivo* PET molecular imaging. PET images were acquired with a YAP-(S)-PET II small animal scanner, as previously described. For the shifting to PET modality, we needed to remove the high resolution collimator, maintaining the same setting condition. Three mice per group of treatment were anaesthetized with a mixture of 4 % isoflurane in air, and were injected intravenously with 3.7 MBq of [^{18}F]FDG. After 1 h from the injection, the mice were positioned prone on the PET/SPECT scanner bed with the tumour centred in the field of view (FOV). Dynamic PET data were acquired for 30 minutes (six scans of 5 minutes). The first PET analysis was performed the day before the beginning of treatment and remade every three weeks. PET data were acquired in list mode, using the full axial acceptance angle of the scanner (3D mode), and then reconstructed with the Expectation Maximization (EM) algorithm. All images were calibrated with a dedicated phantom, corrected for the radionuclide half-life decay and then quantified with PMOD 2.7 software. Regions of interest (ROIs) were drawn on tumour and muscle for all time points. The radioactivity concentration in tumor was calculated as percentage of injected dose per gram of tissue (%ID/g), and expressed as tumor to muscle ratio.

3.18. Statistical analysis

Values are expressed as mean ± SEM. The statistical significance of differences between groups was evaluated with unpaired Student's t-test. A p-value lower than 0.05 was considered significant.

4. Results and Discussion

4.1. In vitro binding specificity of FITC-SiNPs by flow cytometry

Binding selectivity of SiNPs toward $HER2^+$ BC cells was first evaluated by flow cytometry. To validate this system, SK-BR-3 cells were chosen as $HER2^+$ BC model, while HER2-negative ($HER2^-$) MDA-MB-468 cells were used as negative control. To investigate the impact of functionalization on the binding capability of SiNPs, the study was performed comparing SiNP vs SiNP-TZ (Hc-TZ 1:8) and NTA linker conjugated nanoparticles SiNP-NTA vs SiNP-NTA-TZ (Hc-TZ 1:8), as shown in Figure 9. Each kind of nanoconjugate was incubated for different times (20 min, 1 h, 4 h and 24 h) with SK-BR-3 cells and MDA-MB-468 cells. Flow cytometry evidenced a remarkable time-dependent increase of fluorescence signal after incubation of SiNP-TZ or SiNP-NTA-TZ with SK-BR-3 cells (Figure 9, B and D), in comparison to the treatment with non-functionalized nanoparticles SiNP or SiNP-NTA (Fig. 9, A and C). A significant difference ($P<0.05$) occurred when SK-BR-3 incubated with SiNP-TZ or SiNP-NTA-TZ were compared to MDA-MB-468 cells treated with the same nanoparticles. This data demonstrated the capability of targeted SiNPs (SiNP-TZ and SiNP-NTA-TZ) to selectively recognize HER2 receptors in SK-BR-3 cells. SiNP/SiNP-NTA exhibited a remarkably lower uptake in SK-BR-3 cells compared to Hc-TZ-modified SiNPs and no preferential affinity toward SK-BR-3 or MDA-MB-468 cell lines was found (Figure 9, A and C), suggesting that the interaction with cells was essentially attributable to nonspecific uptake in both HER2− and HER2+ lines. However, nonspecific uptake was basically negligible within the first 4 h.

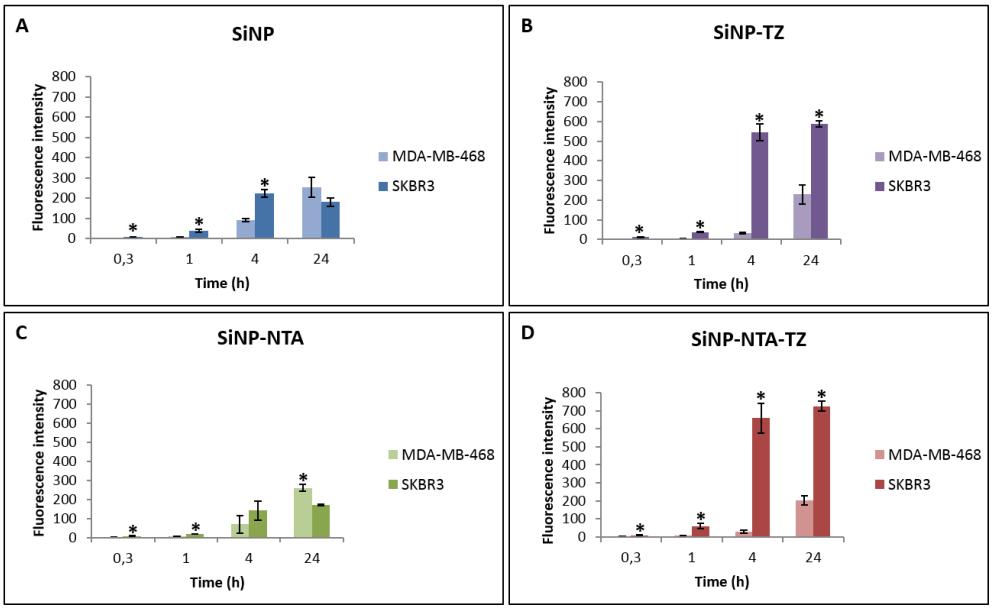

Figure 9. Assessment of binding specificity by flow cytometry. Panels A-D represent the distribution of cell fluorescence intensity, normalized over untreated cells (control), in MDA-MB-468 and SK-BR-3 cell lines after exposure to A) SiNP, B) SiNP-TZ, C) SiNP-NTA and D) SiNP-NTA-TZ at 20 min, 1 h, 4 h and 24 h at a concentration of 50 mg/ml (experiments performed, n = 3). (Student's t-test; *$p < 0.05$ vs. MDA-MB-468)[44]

4.2. In vitro fluorescence microscopy on BC cell lines

To confirm the specificity of binding showed by flow cytometry, the binding of Hc-TZ functionalized SiNPs to $HER2^+$ cells was assessed by fluorescence microscopy. SiNP, SiNP-TZ (1:8 Hc-TZ), SiNP-NTA and SiNP-NTA-TZ (1:8 Hc-TZ) were incubated in parallel in SK-BR-3 and MDA-MB-468 cells for 20 min, 1 h, 4 h, 24 h. Fluorescence microscopy images showed that green fluorescence signal started to increase in $HER2^+$ cells 1 h after the incubation with SiNP-NTA-TZ (Figure 10) or SiNP-TZ (Figure 11). In these cells, fluorescence

intensity increased over time, and was considerably stronger than that shown in SiNP-NTA or SiNP images. We did not observe any differences in the behavior of SiNP-NTA-TZ and SiNP-TZ synthetized without NTA linker. In addition, no significant difference for SiNP-NTA or SiNP fluorescence intensity was observed between the cell lines, confirming the loss of SiNPs selectivity in the absence of Hc-TZ conjugation. SK-BR-3 pictures acquired at 4 h and 24 h exhibited a perinuclear localization of green fluorescence signals exclusively after incubation with SiNP-NTA-TZ or SiNP-TZ. In contrast, SiNP-NTA-TZ and SiNP-TZ signals were not found in the cytoplasm of $HER2^{-}$ cells, and remained localized outside the cells after 4 h and 24 h of incubation. At these time points, it was apparent that a large number of SiNP-NTA-TZ and SiNP-TZ were internalized by $HER2^{+}$ SK-BR-3 cells, while they could be hardly taken up by $HER2^{-}$ MDA-MB-468 cells, confirming the specific targeting of Hc-TZ-functionalized SiNPs for $HER2^{+}$ tumor cells.

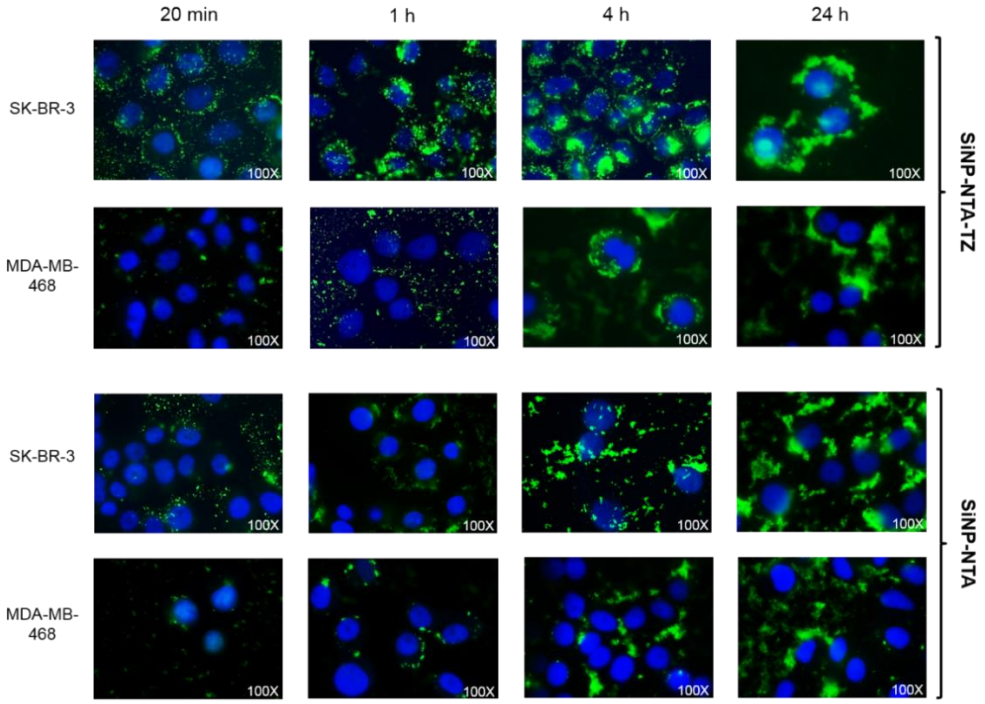

Figure 10. Binding specificity by fluorescence microscopy. SK-BR-3 and MDA-MB-468 cells were grown on coverslips for 24 h and then exposed for 20 min, 1 h, 4 h and 24 h to 50 µg/ml of FITC-labeled (green) SiNPs functionalized with an amount of about eight Hc-TZ per nanoparticle (SiNP-NTA-TZ, 1:8 Hc-TZ) or without Hc-TZ (SiNP-NTA). Nuclei were stained with Hoechst (blue); (experiments performed, n = 4).[44]

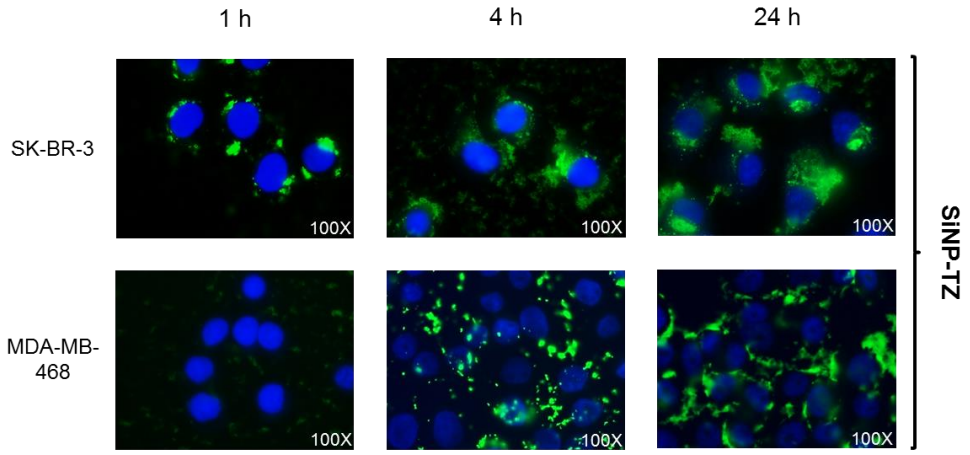

Figure 11. Specificity binding by fluorescence microscopy. SK-BR-3 and MDA-MB-468 cells were grown on coverslips for 24 h and then exposed for 1, 4 and 24 h to 50 µg/ml of FITC-labeled (green) SiNPs, functionalized with Hc-TZ. Nanoparticles were engineered without nitrilotriacetic acid chelating linker for evaluate its contribution on targeting capability. Nuclei were stained with Hoechst (blue); (experiments performed, n = 4).[44]

4.3. In vitro uptake of radiolabeled ^{99m}Tc-SiNP-NTA-TZ

To evaluate the specificity of ^{99m}Tc-labeled NTA-SiNPs toward HER2^{+} cells, we tested the nanoconstructs with or without Hc-TZ in a kinetic binding assay on HER2^{+} SK-BR-3 in comparison to HER2^{-} MDA-MB-468 cells. ^{99m}Tc-labeled SiNP-NTA and SiNP-NTA-TZ (1:8 Hc-TZ) were incubated in both cell lines for 1, 4 and 24 h. At these time points, media were removed and counted using a γ-counter and cells washed, removed and counted to calculate SiNPs uptake as percentage of total radioactivity administered. Specific binding curves were generated as shown in Figure 12. SiNP-NTA bound weakly and nonspecifically to both the MDA-MB-468 and the SK-BR-3 cells, giving a maximum value of 1.4% uptake 24 h after incubation (Figure 12, A). In contrast, SiNP-

NTA-TZ showed an uptake value of 1.6% in SK-BR-3 cells already after 1 h of incubation, reaching 2.3% at 4 h, compared to 1.1% of uptake observed in MDA-MB-468 cells ($P < 0.05$). It is apparent that the specific uptake ratio (SK-BR-3/MDA-MB-468) for SiNP-NTA-TZ was maximum at this time point. The uptake of SiNP-NTA-TZ continued to increase up to 24 h, showing a slight increase in both cell lines and following a similar nonspecific trend; the uptake value reached 3.7% in $HER2^+$ cells and 2.1% in $HER2^-$ cells (Figure 12, B).

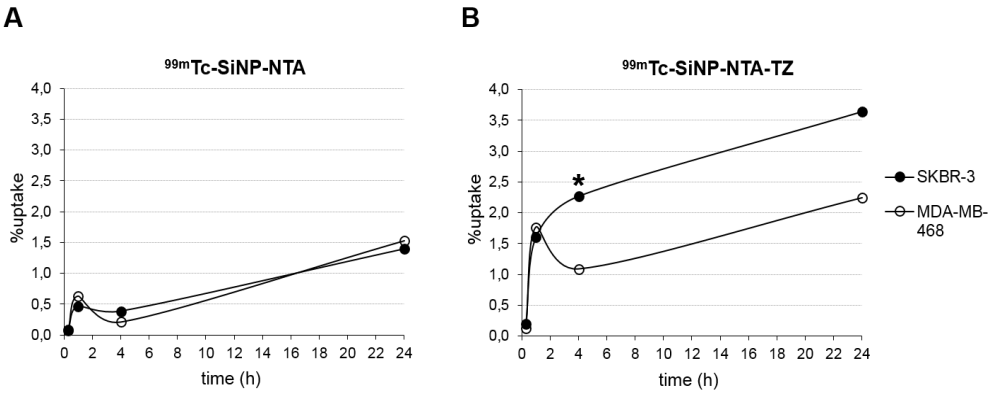

Figure 12. *In vitro* uptake of ^{99m}Tc-radiolabeled A) SiNP-NTA and B) SiNP-NTA-TZ (1:8 Hc-TZ). SK-BR-3 and MDA-MB-468 cells were incubated with SiNPs (1 µCi/ml) for 1, 4, 24 h. Cell uptake was expressed as % of total radioactivity administered (experiments performed, n = 3). (Student's *t*-test; *$p < 0.05$ *vs.* MDA-MB-468)[44]

4.4. Ex vivo biodistribution of ^{99m}Tc-SiNP-NTA-TZ in tumor

Spherical nanoparticle shell was engineered with nitrilotriacetic acid (NTA) liker, in order to radiolabel and follow the nanoparticles shell, for either SiNPs with Hc-TZ (SiNP-NTA-TZ) or without (SiNP-NTA) by nuclear medicine techniques. Biodistribution pattern of ^{99m}Tc-labeled SiNPs (SiNP-NTA and SiNP-NTA-TZ) was assessed in a SK-BR-3

tumor mouse model at 4, 6 and 24 h. The results are summarized in Figure 13. At 4 h after injection of radiolabeled SiNP-NTA-TZ (1:8 Hc-TZ) or SiNP-NTA, radioactivity accumulation in SK-BR-3 tumor was higher for TZ-conjugated SiNPs compared to nontargeted. At this time, mean tumor uptake (expressed as %ID/g) was 0.52 ± 0.08 for SiNP-NTA and 0.67 ± 0.03 for SiNP-NTA-TZ (Fig. 13, A), and ratio tumor-muscle (%ID/g **/** %ID/g) were 1.69 ± 0.18 and 3.45 ± 1.02 for SiNP-NTA and SiNP-NTA-TZ, respectively (Fig. 13, B). At longer times of exposure, we observed a reduction in tumor radioactivity concentration for animals injected with SiNP-NTA-TZ, but not in those injected with SiNP-NTA. The decline of SiNP-NTA-TZ uptake value, observed from 6 h post-injection, could be explained by an active targeting followed by lysosomal degradation and consequent rapid wash out of SiNPs' shell, labeled with ^{99m}Tc. The increase overtime of radioactivity uptake observed in animals injected with SiNP-NTA suggests a passive targeting process, promoted by tumor EPR effect.

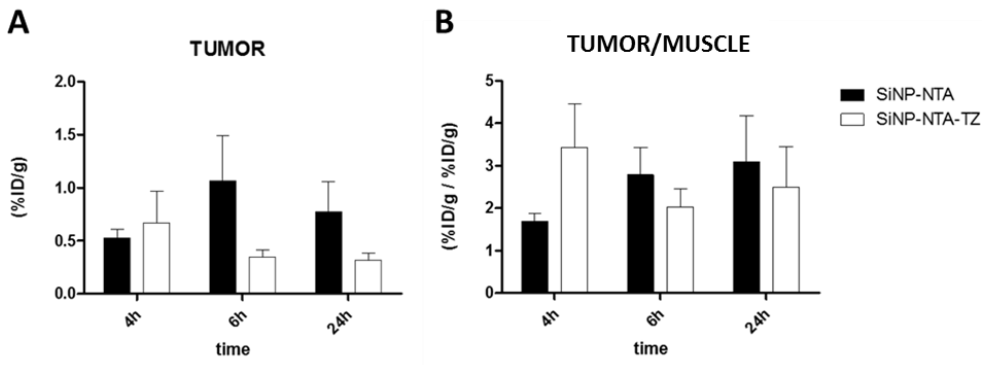

Figure 13. *Ex vivo* biodistribution of ^{99m}Tc-labeled SiNP-NTA and SiNP-NTA-TZ (1:8 Hc-TZ) nanoparticles. SK-BR-3 tumor bearing mice were sacrificed at 4, 6 and 24 h (n = 4) post-injection. Samples were dissected and analyzed

by γ-counter to obtain B) tumor to muscle ratio of %ID/g and A) the tumor absolute values (experiments performed, n = 3). (Student's *t*-test)[44]

4.5. Ex vivo fluorescence microscopy of ^{99m}Tc-SiNP-NTA-TZ in tumor

To better understand the *ex vivo* tumor uptake data, obtained by radioactivity counting, the targeting specificity of ^{99m}Tc-labeled NPs (SiNP-NTA-TZ *vs.* SiNP-NTA) was assessed by post-mortem fluorescence microscopy, in SK-BR-3 lesions. After radioactivity decay, immunofluorescence staining of tumor cryosections, collected 4 h post-injection, allowed us to establish the distribution of the two nanotracers (Figure 14). Images of SiNPs (green) and β-actin (red) were overlaid on the corresponding images reporting nuclei (blue). Green fluorescence intensity in SiNP-NTA-TZ images was significantly higher than that showed from SiNP-NTA and it was mainly colocalized in the perinuclear area. The green fluorescence distribution in SiNP-NTA images was barely detectable on the surface of SK-BR-3 tumor cell membrane, confirming the radioactivity biodistribution results at 4 h.

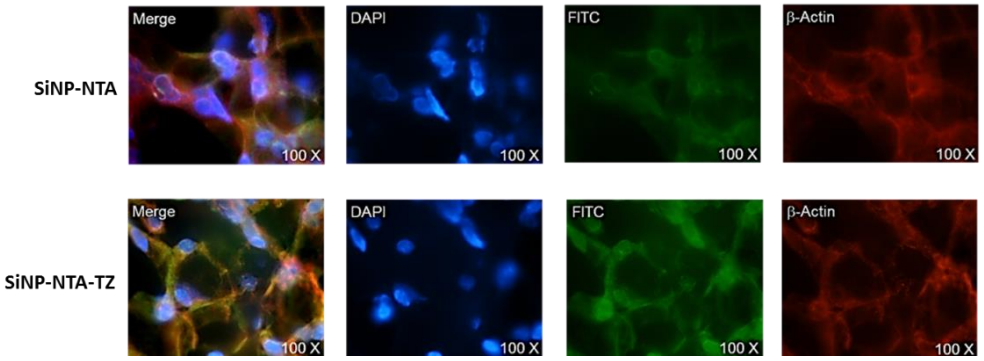

Figure 14. *Ex vivo* immunofluorescence of SK-BR-3 tumor cryosections collected at 4 h post-injection of SiNP-NTA (top) and SiNP-NTA-TZ (bottom).

Merge images represent the colocalization of SiNPs (green), β-actin (red) and reporting nuclei (blue); (experiments performed, n = 3).[44]

4.6. Ex vivo biodistribution of ^{99m}Tc-SiNP-TZ (1:2 and 1:8 Hc-TZ) in tumor

SiNP-TZ nanoparticles, realized without NTA linker, were radiolabeled directly on histidine (His) residues of Hc-TZ, in order to evaluate also the distribution of this component *in vivo/ex vivo* and for simplify the radiolabeling procedure. In a recent study by Colombo *et al.*[64], the authors demonstrated in HER2 positive breast cancer models that tumor targeting and therapeutic effect of spherical nanoparticles depend on the number of attached antibodies; then reducing the antibodies is possible to improve the efficiency. For this reason, we reduced the amount of Hc-TZ conjugated to SiNPs shell, decreasing the Hc-TZ dose during the reaction to a quarter than that previously used for nanoparticle synthesis. This, in order to get about two Hc-TZ (1:2 Hc-TZ) per SiNP. Biodistribution kinetic of ^{99m}Tc-labeled SiNP-TZ (1:2 and 1:8 Hc-TZ) was assessed in a SK-BR-3 tumor mouse model at 1, 4, 6 and 24 h. At 1h and 4 h after injection of radiolabeled SiNP-TZ (1:2 Hc-TZ), radioactivity accumulation in SK-BR-3 tumor seemed higher compared to SiNP-TZ (1:8 Hc-TZ), although not significant (Fig. 15). At this times, mean tumor uptake (expressed as %ID/g) was 0.40 ± 0.05 and 0.57 ± 0.15 for SiNP-TZ (1:2 Hc-TZ) respectively, whereas it was 0.31 ± 0.06 and 0.51 ± 0.34 for SiNP-TZ (1:8 Hc-TZ) (Fig. 15, A). At 1 and 4 h, tumor to muscle ratios of %ID/g were 2.89 ± 0.84 and 3.24 ± 0.22 for SiNP-TZ (1:2 Hc-TZ), and 2.24 ± 0.48 and 2.58 ± 0.73 for SiNP-TZ (1:8 Hc-TZ) (Fig. 15, B). At 6 h, SiNP-TZ (1:8 Hc-TZ) showed an increase of uptake expressed as ratio values (3.31 ± 0.82)

in comparison to SiNP-TZ (1:2 Hc-TZ) (2.83 ± 0.47). At 24 h, the uptake values did not change for both the nanoparticles, with a slight not significant decrease of SiNP-TZ (1:2 Hc-TZ), confirming the presence of radiolabeled Hc-TZ to the tumor, throughout the experimental period. These uptake results of SiNP-TZ (1:8 Hc-TZ), radiolabeled by Hc-TZ direct method, reversed the trend showed at longer times (6 and 24 h) by the nanoparticles labelled via NTA method. The decline of SiNP-NTA-TZ (1:8 Hc-TZ) uptake value, as previously suppose, might be due to an active targeting followed by lysosomal degradation and consequent rapid wash out of SiNPs shell labeled with ^{99m}Tc. For these reason, SiNP-TZ (1:8 Hc-TZ) was chosen for further evaluation *in vitro and ex vivo/in vivo*.

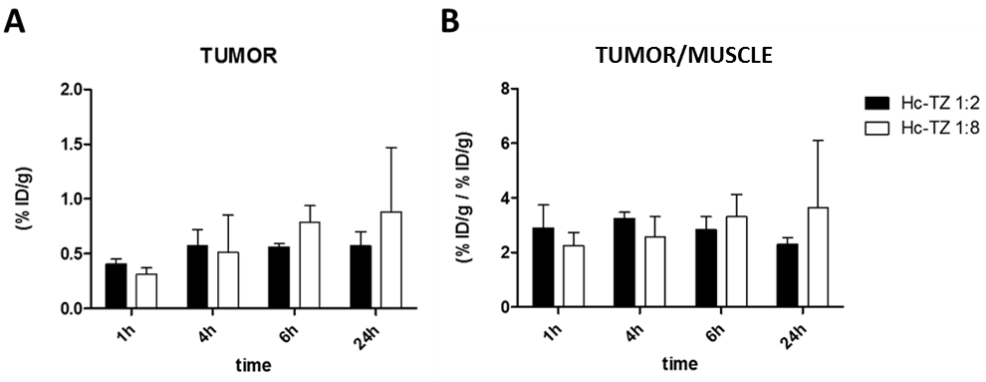

Figure 15. *Ex vivo* biodistribution of ^{99m}Tc-labeled SiNP-TZ (1:2 Hc-TZ) and SiNP-TZ (1:8 Hc-TZ) nanoparticles. SK-BR-3 tumor bearing mice were sacrificed at 1, 4, 6 and 24 h (n = 4) post-injection. Samples were dissected and analyzed by γ-counter to obtain B) tumor to muscle ratio of %ID/g and A) the tumor absolute values (experiments performed, n = 3). (Student's *t*-test)

4.7. In vivo SPECT kinetic study

We performed a preliminary *in vivo* SPECT kinetic evaluation of SiNP-TZ (1:8 Hc-TZ) biodistribution, using a xenograft HER2+ tumor mouse. SPECT images examined after nanoparticles injection showed that radioactivity accumulates immediately in tumor at 1 h, remarkable with a high increase at 4 h (Figure 16). At 24 h post injection, the radioactivity not was detectable by SPECT imaging technique, due to decay. This results are promising for *in vivo* non-invasive detection of HER2 positive breast cancer lesions.

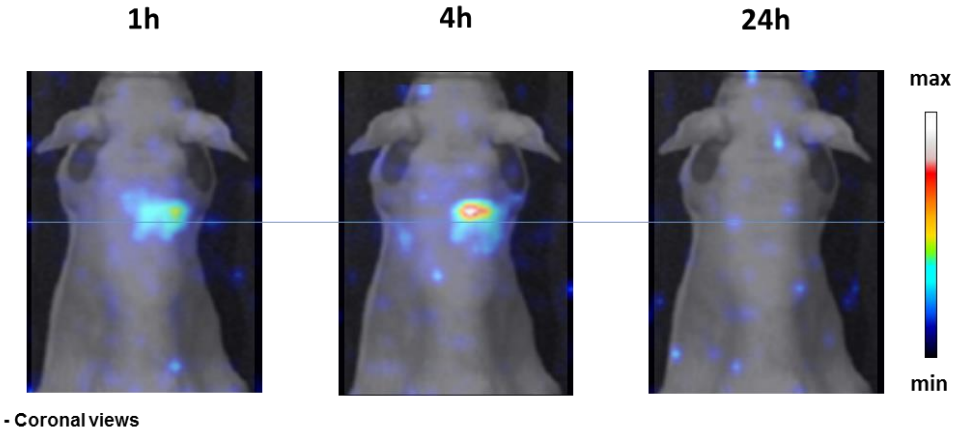

Figure 16. *In vivo* SPECT images of a mouse injected with radiolabelled SiNP-TZ (1:8 Hc-TZ) at 1, 4 and 24 h post injection. Each acquisitions were showed in coronal sections, mouse were anaesthetized with a mixture of 4 % isoflurane in air and injected intravenously with 6,5 MBq of ^{99m}Tc-SiNP-TZ (1:8 Hc-TZ). The blue line highlight the tumor level, an optical image of mouse was merged as anatomical reference (experiments performed, n = 1).

4.8. In vitro evaluation of doxorubicin delivery by DOX-SiNPs

For cancer therapy it is essential to deliver drugs to specific cancer cells. For *in vitro* tests, SK-BR-3 cell line was chosen as a tumor cell

model. As a negative control, MCF-10A cell line was introduced. DOX loaded nanoparticles (DOX-SiNP and DOX-SiNP-TZ, 1:8 Hc-TZ) were used as carrier and cell selectivity was evaluated by fluorescent confocal microscopy. As shown in Fig. 17, A, SK-BR-3 cells incubated with targeted nanoparticles DOX-SiNP-TZ, for 1 h, showed a red fluorescence signal much stronger than those incubated with DOX-SiNP (Fig. 17, B). It should be noticed that DOX carried by DOX-SiNP-TZ was internalized by HER2-overexpressing SK-BR-3 cells, conversely to the DOX-SiNP nanoparticles. Meanwhile, in normal MCF-10A cells DOX diffusion by DOX-SiNP-TZ was lower, suggesting that this system own a satisfactory specificity to HER2-positive tumor cells.

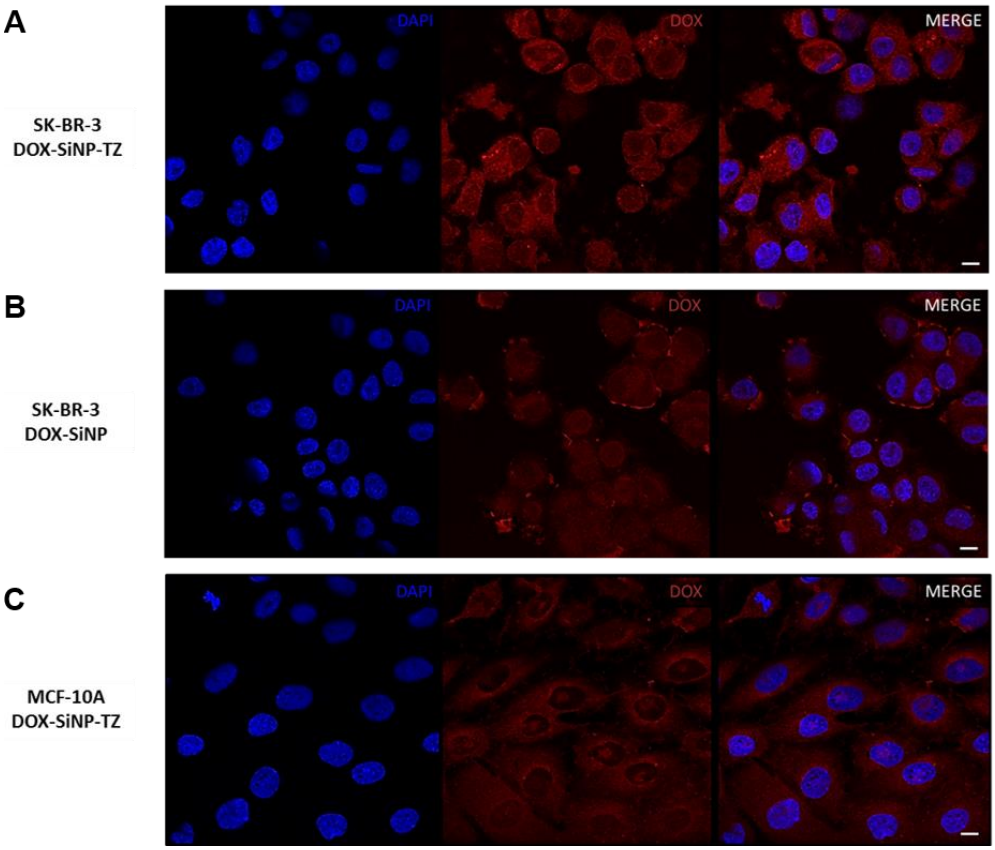

Figure 17. The cellular uptake was imaged by confocal microscopy, following treatment with A) SiNPs-DOX and B) SiNPs-DOX-TZ nanoparticles in SK-BR-3 BC and C) normal MCF-10A cells (experiments performed, n = 1). (Scale bar: 10 μm)

4.9. In vivo evaluation of doxorubicin delivery by DOX-SiNPs

To confirm the targeting ability of the drug delivery system *in vivo,* fluorescence images of SK-BR-3 tumor-bearing mice were captured after intravenous injection of DOX-SiNP-TZ (1:8 Hc-TZ). At 6 h, different nanoparticles formulation were assayed by Optical Imaging: Caelyx, DOX-SiNP and DOX-SiNP-TZ. BC is a superficial localized tumor; the whole-body images could be used for observation of relative

distribution of DOX within tumor sites compared to the other tissues (Fig. 18, A). Images of DOX-SiNP-TZ injected mice, showed an increase of DOX accumulation to the tumor in comparison to the DOX-SiNP, similarly to Caelyx. Fluorescent quantification of excised tumors and tissues images (Fig. 18, B), at 6 h p.i., expressed as tissues to muscle ratios (Fig. 18, D), confirmed this result. In peripheral district, all nanoparticles formulations shown accumulation mainly in liver and kidney, elimination organs.

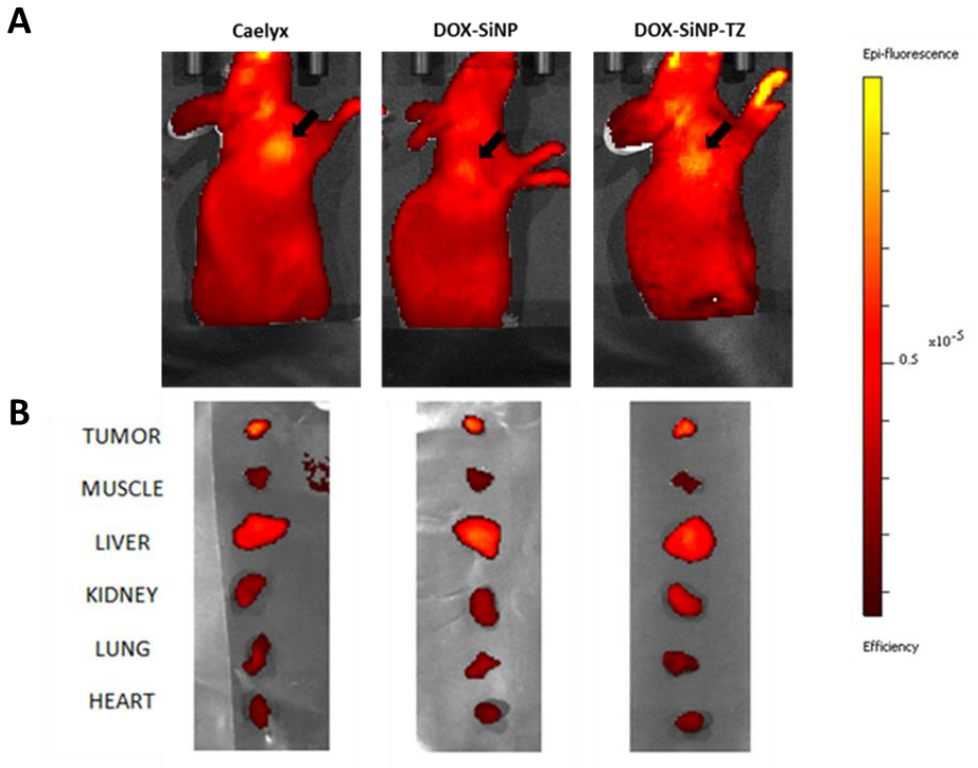

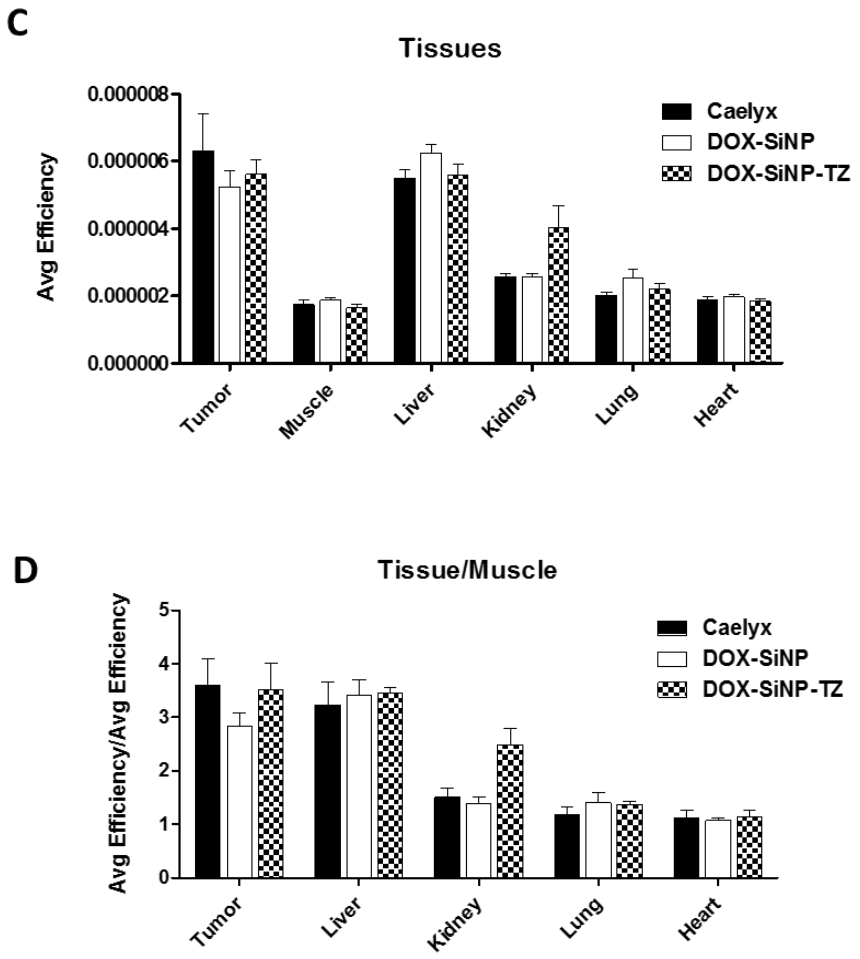

Figure 18. A) Fluorescent imaging *in vivo* and *ex vivo* biodistribution at 6 h of Caelyx, DOX-SiNP and DOX-SiNP-TZ nanoparticles, loaded with DOX (Ex.480 nm/Em.580 nm), at and 6 h post i.v. administration in mice bearing SK-BR-3 tumors. Black arrows indicate the tumors. B) Ex vivo fuorescent biodistribution of DOX, in peripheral district, carried by four different nanoparticle formulations (at 6 h post injection). C) *Ex vivo* fluorescent biodistribution for each nanoparticle set in SK-BR-3 tumor bearing mice (n = 3 mice per group), sacrificed at 6 h post-injection. Samples were dissected and analyzed IVIS Spectrum in vivo imaging system at selected time points (1, 4 and 6 h) and the results are expressed as Avenger Efficiency of

fluorescence emission, D) the biodistribution values, at the same experimental time, are expressed as samples to muscle ratio of Avenger Efficiency of fluorescence emission (experiments performed, n = 1). (Student's *t*-test)

4.10. In vivo evaluation of treatment efficacy of DOX-SiNPs and Caelyx

Female Balb/c nude mice were randomized when tumor volumes reached an average of 100 mm^3 and subdivided into 4 treatment groups (Control: n. 5 mice; Caelyx: n. 9 mice; DOX-SiNP: n. 6 mice and DOX-SiNP-TZ: n. 8 mice). Mice were weekly injected i.v. with a dose of 1mg/Kg of DOX loaded by several nanoparticles formulation for six weeks of treatment. Efficacy of treatment was assessed *in vivo,* monitoring twice a week the tumor volume. At the end of treatment, the animals displayed a decrease in tumor volume, compared to control animals (Fig. 19): the highest inhibitory effect (57.2 %) was observed for SiNP-TZ (1:8 Hc-TZ), with significant results ($p < 0.001$) in comparison to Caelyx (35.2 %) and non targeted nanoparticles SiNP (33.5 %). In addition, the response to treatment was assessed evaluating glucose tumor metabolism, monitoring [^{18}F]FDG tumor uptake by *in vivo* PET imaging. PET images were acquired the day before the treatment started, after three and six weeks. In Figure 20, the results are reported as tumor to muscle ratio. No significant differences were observed at [^{18}F]FDG-PET. Tumor uptake showed a reduction only after three weeks of treatment with SiNP-TZ (1:8 Hc-TZ) in comparison to control group, where the values remain steady over time, as well as for SiNP group. Caelyx group showed a transient

increase of [^{18}F]FDG tumor uptake at three weeks of treatment that decreased at six weeks, reaching to control group values.

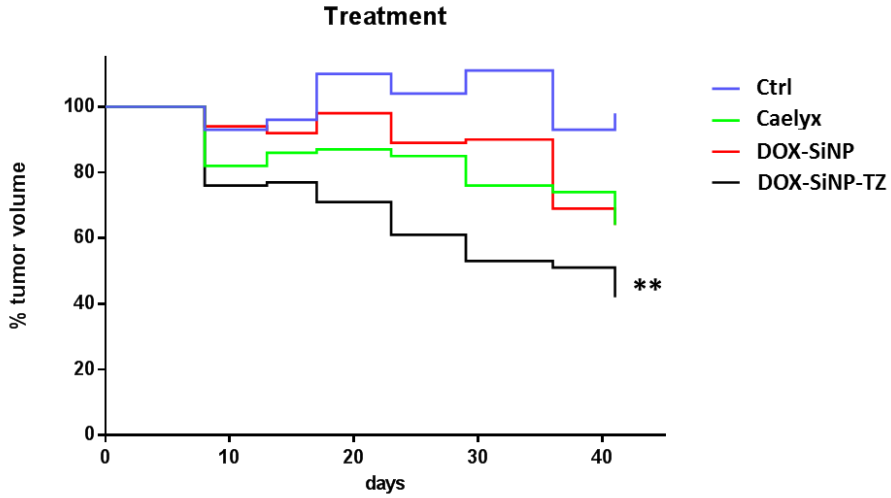

Figure 19. Treatment efficacy results expressed as percentage of tumor volume reduction. Four treatment groups (Ctrl: n. 5 mice; Caelyx: n. 9 mice; DOX-SiNP: n. 6 mice and DOX-SiNP-TZ: n. 8 mice). Mice were weekly-injected i.v. with a dose of 1mg/Kg of doxorubicin loaded by both several nanoparticles formulation, for six weeks of treatment (experiments performed, n = 1). (Student's *t*-test; **p < 0.001 *vs.* Caelyx)

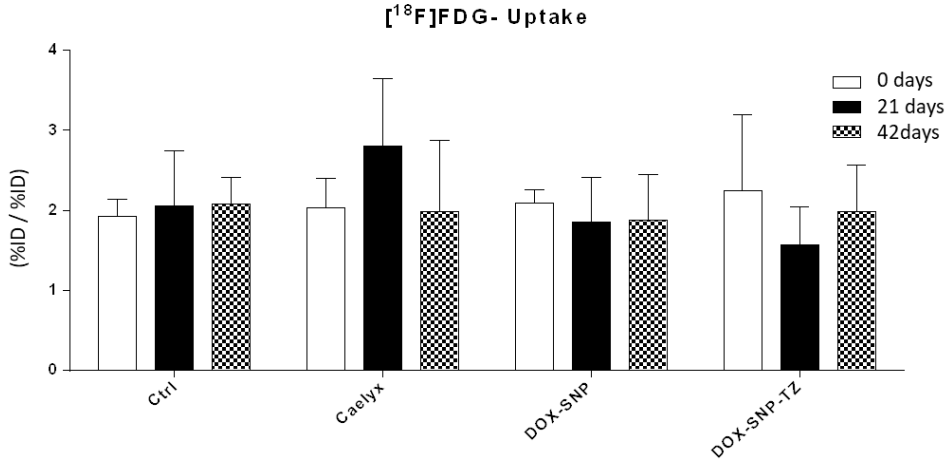

Figure 20. Treatment efficacy evaluation by [^{18}F]FDG tumor uptake. Three

mice per group were intravenously injected with 3.7 MBq of [^{18}F]FDG and 1 h post injection were acquired. The radioactivity concentration in tumor was calculated as percentage of injected dose per gram of tissue (%ID/g) and expressed as tumor to muscle ratio (experiments performed, n = 3). (Student's *t*-test)

5. Conclusion and perspective

At present, the detection of HER2 in BC and in its metastases is based on anatomical imaging technique with several limitation in sensitivity and specificity. Moreover phenotype assessment is performed by invasive methods as biopsy, to obtain representative tissue for immunohistochemistry analysis.[65] Recently, new approaches are developed to determine soluble markers, such as HER2 extracellular domain and circulating miRNA for patients' stratification, but these strategies have not been standardized yet.[66,67] To overcome the current limitations, the present Thesis evaluated the potential use of a multifunctional silica nanoparticles (SiNPs) based system, able to acts as a PET/SPECT radiotracer for tumor detection and as chemotherapy drug carrier, opening the opportunity to develop a new generation of theranostic[68] agents, for noninvasive detection and treatment of HER2+ tumor lesions. This radiolabeled system, in *in vitro* previous to doxorubicin loading tests, not only exhibited low toxicity[44] (data not shown, published in manuscript Rainone *et al.*) and an enhanced targeting for the tumor, compared to passive diffusion, but also significantly increased the selective accumulation of SiNPs within the $HER2^{+}$ SK-BR-3 cells. In fact, takes advantage of an optimized conjugation to the half-chain fragment of the humanized antibody TZ, already in use in the clinical practice.[69] The first radiolabeling procedure tested, was performed through the radioligand-NTA complex and was important to follow both SiNP-NTA and SiNP-NTA-TZ, in order to assess the active targeting contribution offered by antibody chain Hc-TZ. The second radiolabeling method, directly introduce the radioisotope on the antibody chain of Hc-TZ on SiNP-

TZ, in order to follow the fate of the nanoconjugate components separately and to simplify the nanoparticles synthesis and labeling procedure. Taken together, *ex vivo/in vivo* biodistribution results confirmed a good specificity of radiolabeled ^{99m}Tc-SiNP-TZ in the detection of HER2 positive breast cancer lesions, and have led to choose SiNP-TZ (1:8 Hc-TZ), functionalized with eight half-chain of TZ, for further investigations. Doxorubicin loaded nanoparticles, *in vitro* and *ex vivo/in vivo* diffusion assay, confirmed a good specificity of DOX delivery by SiNP-TZ, which resulted similar to the clinical gold standard Caelyx. Preliminary *in vivo* treatment evaluation, showed an improved efficacy of doxorubicin loaded nanoparticles DOX-SiNP-TZ in tumor volume reduction, in comparison to non-targeted DOX-SiNP and Caelyx. This promising efficacy results, could be due to the active internalization of DOX in cancer cells by targeted nanoparticles SiNP-TZ in comparison to the others two non-specific delivery system (SiNP and Caelyx). Moreover, *in vitro* and *ex vivo* proteomics assay are ongoing in order to investigate the different activated pathways, involved in nanoparticles antiblastic activity. Although preliminary results are encouraging, further *in vivo* efficacy and toxicity evaluations are needed to promote the potential use of SiNPs-TZ as a new theranostic agent, for noninvasive detection and treatment of HER2 positive breast cancer.

6. References

1 **Youlden, D. R. *et al.* The descriptive epidemiology of female breast cancer: an international comparison of screening, incidence, survival and mortality. *Cancer Epidemiol* 36, 237-248, doi:10.1016/j.canep.2012.02.007 S1877-7821(12)00029-X [pii] (2012).**

2 **Fisher, B. *et al.* Twenty-year follow-up of a randomized trial comparing total mastectomy, lumpectomy, and lumpectomy plus irradiation for the treatment of invasive breast cancer. *N Engl J Med* 347, 1233-1241, doi:10.1056/NEJMoa022152 347/16/1233 [pii] (2002).**

3 **Bray, F. *et al.* Global cancer statistics 2018: GLOBOCAN estimates of incidence and mortality worldwide for 36 cancers in 185 countries. *CA Cancer J Clin* 68, 394-424, doi:10.3322/caac.21492 (2018).**

4 **DeSantis, C., Ma, J., Bryan, L. & Jemal, A. Breast cancer statistics, 2013. *CA Cancer J Clin* 64, 52-62, doi:10.3322/caac.21203 (2014).**

5 **Greaney, M. L. *et al.* Study protocol for Young & Strong: a cluster randomized design to increase attention to unique issues faced by young women with newly diagnosed breast cancer. *Bmc Public Health* 15, doi:ARTN 37 10.1186/s12889-015-1346-9 (2015).**

6 **Lee, H. B. & Han, W. Unique features of young age breast cancer and its management. *J Breast Cancer* 17, 301-307, doi:10.4048/jbc.2014.17.4.301 (2014).**

7 **Jafari, S. H. *et al.* Breast cancer diagnosis: Imaging techniques and biochemical markers. *J Cell Physiol* 233, 5200-5213, doi:10.1002/jcp.26379 (2018).**

8 **Jeraj, R., Bradshaw, T. & Simoncic, U. Molecular Imaging to Plan Radiotherapy and Evaluate Its Efficacy. *Journal of nuclear***

medicine : official publication, Society of Nuclear Medicine **56, 1752-1765, doi:10.2967/jnumed.114.141424 (2015).**

9 Schmidt, C. Immunology: Another shot at cancer. *Nature* 527, S105-S107, doi:10.1038/527S105a (2015).

10 Viale, G. The current state of breast cancer classification. *Ann Oncol* 23, 207-210, doi:10.1093/annonc/mds326 (2012).

11 Koboldt, D. C. *et al.* Comprehensive molecular portraits of human breast tumours. *Nature* 490, 61-70, doi:10.1038/nature11412 (2012).

12 Santagata, S. *et al.* Taxonomy of breast cancer based on normal cell phenotype predicts outcome. *J Clin Invest* 124, 859-870, doi:10.1172/JCI70941 (2014).

13 Curtis, C. *et al.* The genomic and transcriptomic architecture of 2,000 breast tumours reveals novel subgroups. *Nature* 486, 346-352, doi:10.1038/nature10983 (2012).

14 Gianni, L. *et al.* 5-year analysis of neoadjuvant pertuzumab and trastuzumab in patients with locally advanced, inflammatory, or early-stage HER2-positive breast cancer (NeoSphere): a multicentre, open-label, phase 2 randomised trial. *Lancet Oncol.* 17, 791-800, doi:10.1016/S1470-2045(16)00163-7 (2016).

15 Greenlee, H. *et al.* Clinical Practice Guidelines on the Evidence-Based Use of Integrative Therapies During and After Breast Cancer Treatment. *Ca-Cancer J Clin* 67, 195-232, doi:10.3322/caac.21397 (2017).

16 Perou, C. M. *et al.* Molecular portraits of human breast tumours. *Nature* 406, 747-752, doi:10.1038/35021093 (2000).

17 Sorlie, T. *et al.* Gene expression patterns of breast carcinomas distinguish tumor subclasses with clinical implications. *Proc Natl*

Acad Sci U S A **98, 10869-10874, doi:10.1073/pnas.191367098 (2001).**

18 Weigelt, B., Peterse, J. L. & van 't Veer, L. J. Breast cancer metastasis: markers and models. *Nat. Rev. Cancer* 5, 591-602, doi:10.1038/nrc1670 (2005).

19 Perez, E. A., Cortes, J., Gonzalez-Angulo, A. M. & Bartlett, J. M. HER2 testing: current status and future directions. *Cancer Treat Rev* 40, 276-284, doi:10.1016/j.ctrv.2013.09.001 (2014).

20 Gerber, B. *et al.* Perioperative screening for metastatic disease is not indicated in patients with primary breast cancer and no clinical signs of tumor spread. *Breast Cancer Res Tr* 82, 29-37, doi:10.1023/B:BREA.0000003917.05413.ac (2003).

21 Allred, D. C. *et al.* Overexpression of HER-2/neu and its relationship with other prognostic factors change during the progression of in situ to invasive breast cancer. *Hum Pathol* 23, 974-979, doi:0046-8177(92)90257-4 [pii] (1992).

22 Siegel, R. L., Miller, K. D. & Jemal, A. Cancer statistics, 2015. *CA Cancer J Clin* 65, 5-29, doi:10.3322/caac.21254 (2015).

23 Slamon, D. J. *et al.* Use of chemotherapy plus a monoclonal antibody against HER2 for metastatic breast cancer that overexpresses HER2. *New Engl J Med* 344, 783-792, doi:Doi 10.1056/Nejm200103153441101 (2001).

24 Moasser, M. M. The oncogene HER2: its signaling and transforming functions and its role in human cancer pathogenesis. *Oncogene* 26, 6469-6487, doi:10.1038/sj.onc.1210477 (2007).

25 GrausPorta, D., Beerli, R. R., Daly, J. M. & Hynes, N. E. ErbB-2, the preferred heterodimerization partner of all ErbB

receptors, is a mediator of lateral signaling. *Embo J* 16, 1647-1655, doi:DOI 10.1093/emboj/16.7.1647 (1997).

26 Citri, A. & Yarden, Y. EGF-ERBB signalling: towards the systems level. *Nat Rev Mol Cell Biol* 7, 505-516, doi:10.1038/nrm1962 (2006).

27 Linggi, B. & Carpenter, G. ErbB receptors: new insights on mechanisms and biology. *Trends Cell Biol* 16, 649-656, doi:10.1016/j.tcb.2006.10.008 (2006).

28 Schneeweiss, A. *et al.* Pertuzumab plus trastuzumab in combination with standard neoadjuvant anthracycline-containing and anthracycline-free chemotherapy regimens in patients with HER2-positive early breast cancer: a randomized phase II cardiac safety study (TRYPHAENA). *Annals of oncology : official journal of the European Society for Medical Oncology* 24, 2278-2284, doi:10.1093/annonc/mdt182 (2013).

29 Chang, H. R. Trastuzumab-based neoadjuvant therapy in patients with HER2-positive breast cancer. *Cancer* 116, 2856-2867, doi:10.1002/cncr.25120 (2010).

30 Hynes, N. E. & Lane, H. A. ERBB receptors and cancer: the complexity of targeted inhibitors. *Nat. Rev. Cancer* 5, 341-354, doi:10.1038/nrc1609 (2005).

31 Murthy, R. K. *et al.* Effect of adjuvant/neoadjuvant trastuzumab on clinical outcomes in patients with HER2-positive metastatic breast cancer. *Cancer* 120, 1932-1938, doi:10.1002/cncr.28689 (2014).

32 Gianni, L. *et al.* Efficacy and safety of neoadjuvant pertuzumab and trastuzumab in women with locally advanced, inflammatory, or early HER2-positive breast cancer (NeoSphere): a randomised multicentre, open-label, phase 2 trial. *Lancet Oncol.* 13, 25-32, doi:10.1016/S1470-2045(11)70336-9 (2012).

33 Gianni, L., Salvatorelli, E. & Minotti, G. Anthracycline cardiotoxicity in breast cancer patients: synergism with

trastuzumab and taxanes. *Cardiovasc Toxicol* 7, 67-71, doi:CT:7:2:67 [pii] 10.1007/s12012-007-0013-5 (2007).

34 Barenholz, Y. Doxil(R)--the first FDA-approved nano-drug: lessons learned. *Journal of controlled release : official journal of the Controlled Release Society* 160, 117-134, doi:10.1016/j.jconrel.2012.03.020 (2012).

35 von Minckwitz, G. *et al.* Optimizing taxane use in MBC in the emerging era of targeted chemotherapy. *Crit Rev Oncol Hemat* 85, 315-331, doi:10.1016/j.critrevonc.2012.09.009 (2013).

36 Hurvitz, S. A. *et al.* Neoadjuvant trastuzumab, pertuzumab, and chemotherapy versus trastuzumab emtansine plus pertuzumab in patients with HER2-positive breast cancer (KRISTINE): a randomised, open-label, multicentre, phase 3 trial. *Lancet Oncol.* 19, 115-126, doi:10.1016/S1470-2045(17)30716-7 (2018).

37 Hurvitz, S. A. *et al.* Phase II randomized study of trastuzumab emtansine versus trastuzumab plus docetaxel in patients with human epidermal growth factor receptor 2-positive metastatic breast cancer. *Journal of clinical oncology : official journal of the American Society of Clinical Oncology* 31, 1157-1163, doi:10.1200/JCO.2012.44.9694 (2013).

38 Schmidt, G. P., Haug, A., Reiser, M. F. & Rist, C. Whole-body MRI and FDG-PET/CT imaging diagnostics in oncology. *Radiologe* 50, 329-338, doi:10.1007/s00117-009-1971-3 (2010).

39 Sai, K. K. S., Zachar, Z., Bingham, P. M. & Mintz, A. Metabolic PET Imaging in Oncology. *Am J Roentgenol* 209, 270-276, doi:10.2214/Ajr.17.18112 (2017).

40 Townsend, D. W. Physical principles and technology of clinical PET imaging. *Ann Acad Med Singapore* 33, 133-145 (2004).

41 Alcantara, D., Leal, M. P., Garcia-Bocanegra, I. & Garcia-Martin, M. L. Molecular imaging of breast cancer: present and

future directions. *Front Chem* 2, 112, doi:10.3389/fchem.2014.00112 (2014).

42 Ahlgren, S. *et al.* Targeting of HER2-expressing tumors with a site-specifically 99mTc-labeled recombinant affibody molecule, ZHER2:2395, with C-terminally engineered cysteine. *Journal of nuclear medicine : official publication, Society of Nuclear Medicine* 50, 781-789, doi:10.2967/jnumed.108.056929 (2009).

43 Gainkam, L. O. *et al.* Comparison of the biodistribution and tumor targeting of two 99mTc-labeled anti-EGFR nanobodies in mice, using pinhole SPECT/micro-CT. *J Nucl Med* 49, 788-795, doi:10.2967/jnumed.107.048538 [pii] (2008).

44 Rainone, P. *et al.* Development of 99mTc-radiolabeled nanosilica for targeted detection of HER2-positive breast cancer. *Int J Nanomedicine* 12, 3447-3461, doi:10.2147/IJN.S129720 (2017).

45 Lim, E. K. *et al.* Nanomaterials for Theranostics: Recent Advances and Future Challenges. *Chem Rev* 115, 327-394, doi:Doi 10.1021/Cr300213b (2015).

46 Arano, Y. Recent advances in 99mTc radiopharmaceuticals. *Ann Nucl Med* 16, 79-93 (2002).

47 Bourzac, K. Nanotechnology: Carrying drugs. *Nature* 491, S58-60, doi:10.1038/491s58a (2012).

48 Zhang, R. X., Wong, H. L., Xue, H. Y., Eoh, J. Y. & Wu, X. Y. Nanomedicine of synergistic drug combinations for cancer therapy - Strategies and perspectives. *Journal of Controlled Release* 240, 489-503, doi:10.1016/j.jconrel.2016.06.012 (2016).

49 Wu, D., Si, M. J., Xue, H. Y. & Wong, H. L. Nanomedicine applications in the treatment of breast cancer: current state of

the art. *Int J Nanomedicine* 12, 5879-5892, doi:10.2147/Ijn.S123437 (2017).

50 Orza, A., Casciano, D. & Biris, A. Nanomaterials for targeted drug delivery to cancer stem cells. *Drug Metab Rev* 46, 191-206, doi:10.3109/03602532.2014.900566 (2014).

51 Bourzac, K. Nanotechnology Carrying Drugs. *Nature* 491, S58-S60 (2012).

52 Maeda, H., Wu, J., Sawa, T., Matsumura, Y. & Hori, K. Tumor vascular permeability and the EPR effect in macromolecular therapeutics: a review. *Journal of controlled release : official journal of the Controlled Release Society* 65, 271-284 (2000).

53 Bertrand, N., Wu, J., Xu, X., Kamaly, N. & Farokhzad, O. C. Cancer nanotechnology: the impact of passive and active targeting in the era of modern cancer biology. *Adv Drug Deliver Rev* 66, 2-25, doi:10.1016/j.addr.2013.11.009 (2014).

54 Lim, E. K. *et al.* Nanomaterials for theranostics: recent advances and future challenges. *Chem Rev* 115, 327-394, doi:10.1021/cr300213b (2015).

55 Choi, H. S. & Frangioni, J. V. Nanoparticles for Biomedical Imaging: Fundamentals of Clinical Translation. *Mol Imaging* 9, 291-310, doi:10.2310/7290.2010.00031 (2010).

56 Chow, E. K. H. & Ho, D. Cancer Nanomedicine: From Drug Delivery to Imaging. *Science Translational Medicine* 5, doi:ARTN 216rv4 10.1126/scitranslmed.3005872 (2013).

57 Vivero-Escoto, J. L., Huxford-Phillips, R. C. & Lin, W. B. Silica-based nanoprobes for biomedical imaging and theranostic

applications. *Chem Soc Rev* 41, 2673-2685, doi:10.1039/c2cs15229k (2012).

58 Fiandra, L. *et al.* Assessing the in vivo targeting efficiency of multifunctional nanoconstructs bearing antibody-derived ligands. *ACS nano* 7, 6092-6102, doi:10.1021/nn4018922 (2013).

59 Benezra, M. *et al.* Multimodal silica nanoparticles are effective cancer-targeted probes in a model of human melanoma. *J Clin Invest* 121, 2768-2780, doi:10.1172/JCI45600 (2011).

60 Kempen, P. J. *et al.* Theranostic Mesoporous Silica Nanoparticles Biodegrade after Pro-Survival Drug Delivery and Ultrasound/Magnetic Resonance Imaging of Stem Cells. *Theranostics* 5, 631-642, doi:10.7150/thno.11389 (2015).

61 Veeranarayanan, S. *et al.* Synergistic targeting of cancer and associated angiogenesis using triple-targeted dual-drug silica nanoformulations for theragnostics. *Small* 8, 3476-3489, doi:10.1002/smll.201200874 (2012).

62 Sun, T. *et al.* Engineered nanoparticles for drug delivery in cancer therapy. *Angew Chem Int Ed Engl* 53, 12320-12364, doi:10.1002/anie.201403036 (2014).

63 Riva, B. *et al.* Impact of the strategy adopted for drug loading in nonporous silica nanoparticles on the drug release and cytotoxic activity. *J Colloid Interface Sci* 519, 18-26, doi:10.1016/j.jcis.2018.02.040 (2018).

64 Colombo, M. *et al.* Tumour homing and therapeutic effect of colloidal nanoparticles depend on the number of attached antibodies. *Nat Commun* 7, 13818, doi:10.1038/ncomms13818 [pii] (2016).

65 Gutierrez, C. & Schiff, R. HER2: biology, detection, and clinical implications. *Arch. Pathol. Lab. Med.* 135, 55-62, doi:10.1043/2010-0454-RAR.1 (2011).

66 Leyland-Jones, B. & Smith, B. R. Serum HER2 testing in patients with HER2-positive breast cancer: the death knell tolls.

Lancet Oncol. **12, 286-295, doi:10.1016/S1470-2045(10)70297-7 (2011).**

67 Graveel, C. R., Calderone, H. M., Westerhuis, J. J., Winn, M. E. & Sempere, L. F. Critical analysis of the potential for microRNA biomarkers in breast cancer management. *Breast cancer* 7, 59-79, doi:10.2147/BCTT.S43799 (2015).

68 Geng, J., Liu, J., Liang, J., Shi, H. & Liu, B. A general approach to prepare conjugated polymer dot embedded silica nanoparticles with a SiO2@CP@SiO2 structure for targeted HER2-positive cellular imaging. *Nanoscale* 5, 8593-8601, doi:10.1039/c3nr02390g (2013).

69 Li, C. *et al.* A novel multivalent (99m)Tc-labeled EG2-C4bpalpha antibody for targeting the epidermal growth factor receptor in tumor xenografts. *Nucl Med Biol* 42, 547-554, doi:10.1016/j.nucmedbio.2015.01.011 S0969-8051(15)00024-4 [pii] (2015).

7. Scientific production

7.1. Publications

- Carpinelli A, Rainone P, Belloli S, Reale Annalisa, Cappelli Andrea, Giuliani Germano, Murtaj Valentina, Coliva Angela, Di Grigoli Giuseppe, Valeri Angela, Gilardi Maria Carla, Gianolli Luigi, Anzini Maurizio, Moresco Rosa Maria. **Radiosynthesis and preclinical evaluation of 11C-VA426, a Cyclooxygenase-2 selective ligand.** Contrast Media Mol. Imaging. 2019, DOI: 10.1155/2019/5823261.
- Turolla EA, Valtorta S, Bresciani E, Fehrentz JA, Giuliano L, Stucchi S, Belloli S, Rainone P, Sudati F, Rizzi L, Molteni L, Verdiè P, Martinez J, Torsello A, Moresco RM, Todde S**. Study of the Tissue Distribution of TLQP-21 in Mice Using [18F]JMV5763, a Radiolabeled Analog Prepared via [18F]Aluminum Fluoride Chelation Chemistry.** Front Pharmacol. 2018 Nov 13;9:1274. doi: 10.3389/fphar.2018.01274. eCollection 2018.
- Loffreda A, Jacchetti E, Antunes S, Rainone P, Daniele T, Morisaki T, Bianchi ME, Tacchetti C, Mazza D. **Live-cell p53 single-molecule binding is modulated by C-terminal acetylation and correlates with transcriptional activity.** Nat Commun. 2017 Aug 22;8(1):313. doi: 10.1038/s41467-017-00398-7.
- Rainone P, Riva B, Belloli S, Sudati F, Ripamonti M, Verderio P, Colombo M, Colzani B, Gilardi MC, Moresco RM, Prosperi D. **Development of 99mTc-radiolabeled nanosilica for**

targeted detection of HER2-positive breast cancer. Int J Nanomedicine. 2017 May 2;12:3447-3461. doi: 10.2147/IJN.S129720. eCollection 2017.

7.2. Congress

- **Nanomedicine2019, Milan (Italy), 2-3 May 2019.**
  Poster Presentation: *Evaluation of Doxorubicin loaded ^{99m}Tc-Nanoparticles for Detection and Treatment of HER2-Positive Breast Cancer.* Rainone, P. *et al.*
- **International conference on Bio-Sensing and Imaging – ICOBSI 2018, Florence (Italy), 17-19 December 2018.**
  Poster Presentation: *Evaluation of Doxorubicin loaded ^{99m}Tc-Nanoparticles for Detection and Treatment of HER2-Positive Breast Cancer.* Rainone, P. *et al.*
- **13th National Congress of the Italian Association of Nuclear Medicine and Molecular Imaging – AIMN 2017, Rimini (Italy), 2-5 March 2017.**
  Poster Presentation*: ^{99m}Tc-tricarbonyl Radiolabeled Nanosilica for Targeted Detection of HER2-Positive Breast Cancer.*
  Rainone, P. *et al.*

8. Acknowledgments

This work was supported by a grant from the MIUR, NanoBreastImaging “Progetto Bandiera NanoMAX”.

For this work I want to thank my co-tutor, Dr. Sara Belloli for the supervision during these 3 years of PhD; my tutor, Prof. Maria Alfonsina Desiderio for the opportunity to work in molecular pathology laboratory; Dr. Davide Mazza and Dr. Antonello Spinelli, of Experimental Imaging Centre (CIS) - San Raffaele Scientific Institute, for confocal microscopy images and optical imaging acquisitions.

This thesis was evaluated by two independent reviewers:
<Prof. Emanuele Albano, Professor in General Pathology, Dept. of Health Sciences, University of East Piedmont, Novara>;
<Prof. Rosa Maria Moresco, Professor in N6/01-MED50, Dept. of Medicine and Surgery, University of Milano-Bicocca, Milano>; and by one anonymous reviewer.

9. Research Integrity

Dottorato in Medicina Molecolare e Traslazionale
Dipartimento di Scienze della Salute
Università degli Studi di Milano

LA STATALE

PhD in Molecular and Translational Medicine
Department of Health Science
University of Milan - ITALY

PhD thesis:

^{99m}Tc-Radiolabeled Nanoparticles for Targeted Detection and Treatment of HER2-Positive Breast Cancer

Candidate:

Paolo Rainone

I hereby, Dr. Sara Belloli declare that:

- I am the Co-Tutor of Paolo Rainone for his PhD thesis mentioned above;
- I have read and fully understood the PhD thesis in the current form as of the date below;
- The Candidate and myself are fully aware of the international rules governing authorship in scientific articles and research integrity, as for example those reported in the following web sites:
  - http://www.icmje.org/recommendations/browse/roles-and-responsibilities/defining-the-role-of-authors-and-contributors.html
  - https://www.research-integrity.admin.cam.ac.uk/research-integrity/guidelines/guidelines-authorship
- I did not detect any conflict of interests as for the issues treated in this PhD thesis;
- I did not detect any form of plagiarism nor sign scientific misconduct;
- The research has been carried out following the principles of research integrity;
- I fully endorse the content of this PhD thesis and the underlying message to the scientific community.

Faithfully,

Milano 03.09.2019,

Dr. Sara Belloli

Sara Belloli

Dottorato in Medicina Molecolare e Traslazionale
Dipartimento di Scienze della Salute - Università degli Studi di Milano
Via A. di Rudinì, 8 - 20146 Milano - Italia
Mail: medmol@unimi.it Tel: 02503 23270
Coordinatore: Prof. Michele Samaja (michele.samaja@unimi.it) Segreteria: Morena Urgesi (morena.urgesi@unimi.it)